

12-2016

## Development, Characterization, & Implementation of Phase-Change Material Cold Plates for Hybrid-Electric Vehicle Battery Systems

Kevin Cwiok

Follow this and additional works at: <https://commons.erau.edu/edt>



Part of the [Mechanical Engineering Commons](#), and the [Power and Energy Commons](#)

---

### Scholarly Commons Citation

Cwiok, Kevin, "Development, Characterization, & Implementation of Phase-Change Material Cold Plates for Hybrid-Electric Vehicle Battery Systems" (2016). *Dissertations and Theses*. 295.  
<https://commons.erau.edu/edt/295>

This Thesis - Open Access is brought to you for free and open access by Scholarly Commons. It has been accepted for inclusion in Dissertations and Theses by an authorized administrator of Scholarly Commons. For more information, please contact [commons@erau.edu](mailto:commons@erau.edu).

DEVELOPMENT, CHARACTERIZATION, & IMPLEMENTATION OF  
PHASE-CHANGE MATERIAL COLD PLATES FOR HYBRID-ELECTRIC  
VEHICLE BATTERY SYSTEMS

A Thesis

Submitted to the Faculty

of

Embry-Riddle Aeronautical University

by

Kevin Cwiok

In Partial Fulfillment of the

Requirements for the Degree

of

Master of Science in Mechanical Engineering

December 2016

Embry-Riddle Aeronautical University

Daytona Beach, Florida

DEVELOPMENT, CHARACTERIZATION, & IMPLEMENTATION OF  
PHASE-CHANGE MATERIAL COLD PLATES FOR HYBRID-ELECTRIC  
VEHICLE BATTERY SYSTEMS

by

Kevin Cwiok

A Thesis prepared under the direction of the candidate's committee chairman, Dr. Sandra Boetcher, Department of Mechanical Engineering, and has been approved by the members of the thesis committee. It was submitted to the School of Graduate Studies and Research and was accepted in partial fulfillment of the requirements for the degree of Master of Science in Mechanical Engineering.

THESIS COMMITTEE



Chairman, Dr. Sandra Boetcher



Member, Dr. Patrick Currier



Member, Prof. Rafael Rodriguez



Department Chair, Dr. Charles Reinholtz  
or Graduate Program Coordinator, Dr. Jean-Michel Dhainaut

11/28/16

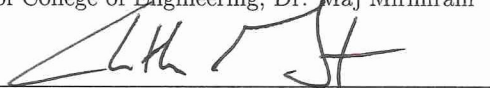
Date



Dean of College of Engineering, Dr. Maj Mirmirani

11/29/2016

Date



Vice Chancellor, Academic Support, Dr. Christopher Grant

11/29/16

Date

## ACKNOWLEDGMENTS

I would like to thank all of my friends and family who have helped me grow throughout my time at Embry-Riddle Aeronautical University. Each challenge and experience has helped push me to become who I am today.

This, of course, would not have been possible without my advisor and friend, Dr. Sandra Boetcher who has offered me direction and inspiration during my career here and onward.

## TABLE OF CONTENTS

	Page
LIST OF TABLES . . . . .	vi
LIST OF FIGURES . . . . .	vii
ABSTRACT . . . . .	x
1 Introduction . . . . .	1
1.1 Modern Battery Systems of Hybrid & Electric Vehicles . . . . .	2
1.1.1 Lithium Ion Batteries . . . . .	2
1.2 Thermal Management Systems . . . . .	4
1.2.1 Air Cooling . . . . .	4
1.2.2 Liquid Cooling . . . . .	5
1.2.3 Phase-Change Material Cooling . . . . .	5
1.3 Thesis Statement . . . . .	6
2 Literature Review . . . . .	7
2.1 PCM Energy Storage . . . . .	7
2.1.1 Latent Heat Storage . . . . .	7
2.1.2 Exploring Thermal Conductivity Enhancers . . . . .	8
2.2 PCM Thermal Management . . . . .	8
2.2.1 Lithium Ion Battery Cooling . . . . .	9
2.2.2 Carbon and Graphite Conductivity Enhancers . . . . .	10
2.3 The Push Into Electric Vehicles . . . . .	11
2.3.1 Electric Vehicle PCM Implementation . . . . .	12
3 Phase-Change Material Modeling & Experimental Testing . . . . .	14
3.1 Test Scope . . . . .	14
3.2 Test Article . . . . .	15
3.3 Test Setup . . . . .	21
3.4 ANSYS Modeling . . . . .	23
4 Discussion of Results . . . . .	28
5 Guarded Hot Plate Apparatus . . . . .	35
5.1 Plate and Tubing Design . . . . .	38
5.1.1 Solution Domain . . . . .	38
5.1.2 Governing Equations, Boundary Conditions, and Initial Condi- tions . . . . .	40
5.1.3 Solution Details . . . . .	42

	Page
5.1.4 Results . . . . .	43
5.2 Tube Configuration Study Using ANSYS CFX . . . . .	51
5.2.1 Solution Domain . . . . .	53
5.2.2 Governing Equations, Boundary Conditions, and Initial Condi- tions . . . . .	53
5.2.3 Solution Details . . . . .	56
5.2.4 Results . . . . .	57
5.3 Final Design . . . . .	58
6 Implementation . . . . .	65
6.1 EcoCAR 3 Competition . . . . .	65
6.2 The Vehicle Test Platform . . . . .	65
6.2.1 PCM Implementation into ESS . . . . .	66
6.2.2 PCM Plate Manufacture . . . . .	67
6.2.3 Vehicle Testing Results . . . . .	69
7 Future Work . . . . .	71
7.1 Shape Stabilized PCM . . . . .	71
7.2 Wax Material Study . . . . .	72
7.2.1 Results . . . . .	74
REFERENCES . . . . .	77

## LIST OF TABLES

Table	Page
3.1 Dimensions of the PCM test sample. . . . .	17
3.2 Dimensions of the PCM top tray. . . . .	18
3.3 Test container dimensions used for the experimental setup . . . . .	19
3.4 Enthalpy values calculated for use in the enthalpy method simulation. .	25
3.5 Material properties of the PCM utilized for numerical modeling. . . . .	25
5.1 Investigated cases for parametric study . . . . .	40
5.2 Material Properties of HDPE and 304 Stainless Steel used for simulations.	41
5.3 Ethylene glycol material properties obtained from MatWeb. . . . .	55
5.4 Mesh independent study element count. . . . .	57
7.1 Wax sample masses used for the DSC experiments. . . . .	74
7.2 Properties obtained from DSC sample testing. . . . .	75

## LIST OF FIGURES

Figure	Page
1.1 Thomas Davenport’s electric vehicle. . . . .	1
3.1 Schematic diagram of the test bench setup. . . . .	16
3.2 Schematic of the PCM plate used for the experiment. . . . .	16
3.3 Aluminum lid piece that is bolted to the aluminum bottom tray. The Southeastern Thermal Systems 40W heater is adhered to the top surface. . . . .	17
3.4 Aluminum support tray and seal design of the PCM test sample. . . . .	18
3.5 Critical locations of the thermocouples used for the test bench experiment. . . . .	19
3.6 PCM test setup with thermocouples embedded in the plate. . . . .	20
3.7 Image of the test bench setup with critical components. . . . .	22
3.8 Heat flux values over the complete E&EC drive cycles of the EcoCAR 2 competition. . . . .	22
3.9 ANSYS APDL model used for the preliminary simulation . . . . .	24
3.10 ANSYS APDL simulation data of bulk PCM-37 to observe the difference in melt characteristics by varying thermal conductivity. . . . .	26
4.1 Heating and melt data observed during the bulk 37 and 48 experiments for thermocouple 2. . . . .	29
4.2 Heating data of the aluminum baseline experiment. . . . .	30
4.3 Temperature versus time of thermocouple 2 data for each of the parametric experiments compared to bulk PCM-37. . . . .	31
4.4 Uneven surface of the 10% sample that was created due to uneven solidification of the PCM. . . . .	32
4.5 The surface of the 1% test sample. Note that it is smooth and without any air pockets. . . . .	32
4.6 Temperature versus time curve of the numerical and experimental comparison. . . . .	33
5.1 Diagram of guarded hot plate test apparatus. . . . .	36



Figure	Page
5.2 Initial tube and plate design. . . . .	38
5.3 Variables to be studied during experiments. . . . .	39
5.4 2D simulation boundary and initial conditions. . . . .	41
5.5 Mesh used for the 2D simulations. . . . .	42
5.6 Temperature contour seen for Case 1. . . . .	44
5.7 Temperature contour for the cold plate of Case 1. . . . .	44
5.8 Temperature contour for the hot plate of Case 1. . . . .	44
5.9 Plot of surface temperatures observed for Case 1. . . . .	45
5.10 Temperature contour seen for Case 2. . . . .	46
5.11 Temperature contour for the cold plate of Case 2. . . . .	46
5.12 Temperature contour for the hot plate of Case 2. . . . .	46
5.13 Plot of surface temperatures observed for Case 2. . . . .	47
5.14 Temperature contour seen for Case 3. . . . .	47
5.15 Temperature contour observed for the cold plate of Case 3. . . . .	48
5.16 Temperature contour observed for the hot plate of Case 3. . . . .	48
5.17 Plot of surface temperatures observed for Case 3. . . . .	49
5.18 Temperature contour of the cold plate for Case 4. . . . .	50
5.19 Temperature contour of the hot plate for Case 4. . . . .	50
5.20 Temperature contour of the cold plate for Case 5. . . . .	51
5.21 Temperature contour of the hot plate for Case 5. . . . .	51
5.23 Schematic of the 3D simulation assembly. . . . .	56
5.24 Contour plot of hot plate surface temperatures. . . . .	58
5.25 Final design of the cold and hot plate. . . . .	60
5.26 Results from the 10 tube 2D simulation. . . . .	60
5.27 Simulation domain for the foam study. . . . .	61
5.28 Temperature contour seen through the thickness of the foam insulation. . . . .	62
5.29 CAD image of the steady state apparatus assembly. . . . .	63
5.30 ANOVA A-40 used for the isothermal plates. . . . .	63

Figure	Page
6.1 ERAU Vehicle Architecture Selection. . . . .	66
6.2 ESS frame design with PCM cold plate trays attached. . . . .	67
6.3 Bottom PCM tray used on the vehicle ESS. . . . .	68
6.4 ESS temperature data obtained during vehicle testing. . . . .	70
7.1 Mettler Toledo Differential Scanning Calorimeter. . . . .	73
7.2 Melt curves of the three sample waxes. . . . .	75

## ABSTRACT

Researcher: Kevin Cwiok

Title: Development, Characterization, & Implementation of Phase-Change Material Cold Plates for Hybrid-Electric Vehicle Battery Systems

Institution: Embry-Riddle Aeronautical University

Degree: Master of Science in Mechanical Engineering

Year: 2016

Due to the regulations on internal combustion engine vehicles, there is a large demand of hybrid and electric vehicles with large battery packs as Energy Storage Systems (ESS) capable of long ranges and decreased emissions. These battery packs output large heat loads during charge-depletion mode and currently require active cooling to keep the batteries within operating conditions. The current systems relied on to achieve this are the air and liquid cooled thermal managements systems. A recent alternative approach to current cooling for ESS thermal management is the use of phase-change materials (PCMs). PCMs regulate the temperature of the ESS by leveraging the latent heat of fusion to absorb large amounts of energy at constant temperature while changing phase from solid to liquid. While PCMs have large heat capacities, the downside is their low thermal conductivity which causes them to melt unevenly, which is a main reason PCM is not ideal for cooling systems. The study will involve fully investigating the use of PCM into a hybrid-electric vehicle battery thermal management system. The proposed methodology is to mix thermal conductivity enhancing material, loose carbon fibers, into the PCM to spread the heat absorbed more evenly throughout the entire mass. This material matrix is characterized in order to determine the necessary material and thermal properties to justify its use and implantation in the EcoEagles 2016 Chevrolet Camaro for vehicle testing and validations. Results obtained during multiple vehicle tests have demonstrated that the PCM has successfully kept the battery pack at a safe operating condition of under 45°C. This was done passively resulting in a reduced overall vehicle energy consumption and increased vehicle battery pack efficiency. The study continues by investigating the use of a shape-stabilized phase-change material cold plate that is capable of addressing several issues that are present with the bulk PCM plate in its current state on the vehicle.

## 1. Introduction

The market for the automotive industry has shifted towards hybridization and electrification of vehicles. Although electric vehicles are more recently available, the first vehicle was developed in 1834 by Thomas Davenport and utilized non-rechargeable batteries (U.S. Department of Energy, The History of the Electric Car). The first successful model with rechargeable batteries was developed in 1891 by William Morrison. In the 1970s through the 90s, the focus on the growing amount of pollution prompted the Pollution Control Act which yielded a stronger interest of electric vehicles (U.S. Environmental Protection Agency, Evolution of the Clean Air Act). Since then, au-



Figure 1.1.: Thomas Davenport's electric vehicle.

tomotive manufacturers have been put under heavy scrutiny for lower emissions and higher fuel economies with the Corporate Average Fuel Economy (CAFE) standards. These regulations are set by the government starting since 1975. CAFE standards state that fleets will have a combined fuel economy of 54.5 miles per gallon and emissions of 163 grams of CO<sub>2</sub> per mile for passenger cars by 2025 (National Highway Traffic Safety Administration, CAFE - Fuel Economy). The major focus is not only to increase energy efficiency of manufacturer's fleets, but to promote advancements in alternative fuels and lower the current vehicle emissions. With the push for these standards, a complete revival of the hybrid and electric vehicle systems are being pushed into the modern market.

## **1.1 Modern Battery Systems of Hybrid & Electric Vehicles**

The modern battery systems used on hybrid and electric vehicles consists of multiple battery modules to create a larger overall system. These modules are comprised of individual battery cells in parallel and series configurations to provide the proper voltage and energy storage for the vehicle to operate.

### **1.1.1 Lithium Ion Batteries**

The current standard for electric vehicles and hybrid electric vehicles is the lithium ion (Li-ion) battery. These batteries are a type of secondary battery that provide high

energy densities, are low maintenance, and are relatively low self-discharging (Battery University, Types of Lithium-ion).

Li-ion cells are capable of yielding over  $200 \frac{Wh}{kg}$  of energy density, which is over double the capacity of similar nickel-cadmium batteries (Battery University, How do Lithium Batteries Work?) . Typical Li-ion batteries have a voltage of 3.6 volts but can also have 3.7 or 3.3 volts. The typical life of a lithium ion battery is between 500 and 2,000 cycles.

#### 1.1.1.1 Lithium Ion Thermal Considerations and Limitations

Although lithium ion batteries provide high energy densities, they are very susceptible to the effects of over heating and thermal runaway. When a Li-ion battery is heated to a temperature of above  $50^{\circ}\text{C}$  ( $122^{\circ}\text{F}$ ) the battery will experience degradation leading to shorter lifespans and charge efficiency (Onda et al, 2006). The overall heat generation from the batteries is calculated using Eq. 1.1.

$$Q_T = Q_r + Q_p + Q_s + Q_J \quad (1.1)$$

In the preceding equation,  $Q_r$  is the reaction heat value,  $Q_p$  is polarization heat loss,  $Q_s$  is side reactions, and  $Q_J$  is Joule heating from the battery. The total heat energy,  $Q_T$ , can be obtained by adding all of these factors together.

For most analyses, the side reaction component of the equation can be considered zero due to the self-discharge or current batteries being low enough to neglect. (Sato, 2001). The remaining three components are considered the major heat contributors to

the battery heat generation. The equations for determining the reaction, polarization, and Joule heating are seen below in Eq. 1.2 - Eq. 1.4.

$$Q_r = 3.73 \times 10^{-2} Q_1 I \quad (1.2)$$

$$Q_p = 3.60 R_p I^2 \quad (1.3)$$

$$Q_J = 3.60 R_e I^2 \quad (1.4)$$

In these equations  $Q_1$  is the total heat generated during the chemical reactions within the lithium ion battery,  $I$  is the current during either charge or discharge,  $R_p$  is the polarization resistance, and  $R_e$  is the electrical resistance of the battery.

## 1.2 Thermal Management Systems

Now that the heat generation of lithium ion batteries is understood, it is important to investigate methods to remove that heat energy through thermal management systems. A thermal management system is commonly used on electronic devices in order to sustain operating temperatures and prevent thermal run-off. These systems can be one of or a mixture of an active system, passive system, or bypass system.

### 1.2.1 Air Cooling

The current and most common battery cooling system in the automotive industry is an active air-cooled system. These systems use air to remove the heat generated through either forced or natural convection. Forced is most common in the automotive industry where the air from the air conditioning fan is forced into the battery container

removing the heat. The natural convection method requires that the battery heat sink be exposed to the environment in order to remove heat during vehicle travel or idle, however, can pose as an issue when exposed to a hot environment. Additionally, the air cooling option is generally cheap and requires minimal parasitic draw to power the pump if the fluid is forced.

### **1.2.2 Liquid Cooling**

Liquid cooling is another common type of cooling system used for battery thermal management. This requires a liquid to be pumped around the batteries in order to remove the heat via a heat exchanger. Liquid is capable of removing more heat more quickly than an air system, but needs more equipment to do it. Furthermore, there is an increased weight associated due to the introduction of the fluid, piping, pump, heat exchanger, and fluid reservoir.

### **1.2.3 Phase-Change Material Cooling**

A recent addition to thermal management is the use of a phase-change material (PCM). PCM is an engineered material capable of storing large amounts of heat energy while changing phase from solid to liquid. PCM absorbs latent heat to change phase while remaining at a specific temperature during the melt. This melt process is similar to what is observed when an ice cube melts. The ice cube will absorb latent



heat energy and remain at a constant  $0^{\circ}\text{C}$  ( $32^{\circ}\text{F}$ ) until it is fully melted where the water will then begin to increase in temperature.

The PCM has many properties that allow it to excel as a thermal management system. It has a large latent heat of fusion,  $210 \frac{\text{J}}{\text{g}}$ , allowing it to absorb a large amount of heat with a small amount of mass. It has a much smaller mass when compared to an aluminum cold plate, at  $\frac{1}{3}$  the density, resulting in an overall light-weight thermal management system. Thus, PCM has become a large topic of research for thermal management systems in everything from portable electronics to full-size vehicles.

### 1.3 Thesis Statement

Although the current air and liquid systems are capable of removing the heat from the batteries effectively, the need to reduce vehicle energy consumption and increase vehicle efficiency is on the rise. These systems have high weights, large power draw, and considerable packaging requirements, but the introduction of a low-mass, passive, and moldable PCM system will address these issues. The purpose of this study is to develop, characterize, and implement a PCM cold plate system that will provide an effective and passive thermal management solution for electric and hybrid-electric vehicle battery systems. The development will include investigations into the increase of thermal conductivity of the material. Characterization will provide necessary material properties needed to finally implement the material into the electric vehicle test platform provided by the universities EcoCAR 3 team.

## 2. Literature Review

### 2.1 PCM Energy Storage

PCM was originally considered as an energy storage system rather than thermal management. Humphries and Griggs (Humphries, 1977) from NASA were some of the first to research phase-change materials for energy storage in the 1970's. This research consisted of a large parametric study of various types of paraffin waxes. They set the baseline for understanding paraffin wax energy storage properties and even the use of thermal conductivity enhancers to alter the material properties.

#### 2.1.1 Latent Heat Storage

Research conducted in the mid 1990's focused on the materials ability to absorb large amounts of latent heat energy and store it for long periods of time. Investigators, Hamdan and Elwerr (Hamdan & Elwerr, 1996), were some of the first to investigate the melt characteristics of phase-change materials. The purpose was to estimate the amount of energy their material could store by observing the melt fraction propagation. Using numerical experiments from previous research, they were able to correlate their data to show that their phase-change material, n-octadecane, was storing the energy as almost 95% latent heat energy and 5% sensible heat energy. This means

that almost 95% of the energy is stored and capable of being pulled from the system and reused.

### **2.1.2 Exploring Thermal Conductivity Enhancers**

Although Humpries and Griggs discussed different thermal conductivity enhancers, it was not until 1999 that Fukai et al (Fukai, Kanou, Kodama, & Miyatake, 2000) investigated the use of a composite material as the additive. The use of the carbon was innovative due to the high thermal conductivity of the carbon fibers combined with the low weight when compared to metal additives. They investigated two methods of mixing the PCM with the carbon fibers, loose fiber additions and a through a structured carbon fiber brush system. Their data showed that by adding as low as 2%, by volume, of carbon into the paraffin wax that the thermal conductivity could increase up to six times that the of the baseline paraffin wax.

## **2.2 PCM Thermal Management**

Using PCM to regulate energy storage system (ESS) temperature was first proposed in 2000 by Al-Hallaj and Selman (Al Hallaj & Selman, 2000), (Al-Hallaj & Selman, 2002). These investigators primarily focused on using PCM inside of the battery between the individual cells of a small electric vehicle battery module. Furthermore, the same researchers were responsible for developing accurate models for PCM thermal management system. They observed that the PCM was not only ca-

pable of absorbing all heat energy generated by the battery, but that it posed a significant advantage for when the batteries were left to relax. The heat that had been stored would transfer into the batteries during charging, which is important for vehicles in cold environments and space applications.

### **2.2.1 Lithium Ion Battery Cooling**

Using the data from Al-Hallaj, Khateeb et al (Khateeb, Farid, Selman, & Al-Hallaj, 2004) took the research a step further and introduced the PCM into a full-scale electric scooter. The scooter selected was the same scooter that Al-Hallaj had taken the batteries from. They decided that the system would be completely passive and rely solely on the PCM for thermal management. During their experiments, it was discovered that the naturally low thermal conductivity of the PCM was limiting the ability to transfer the heat within the material. They investigated the use of aluminum fins and aluminum foam to enhance the low thermal conductivity and low natural convection heat transfer coefficient. It was determined that without the thermal conductivity enhancer, the PCM would be ineffective and cause potential thermal runaway. With the addition of the foam, however, the observed battery temperature decreased by 25°C.

### 2.2.2 Carbon and Graphite Conductivity Enhancers

Due to the success of the thermal management from the scooter battery, Mills et al (Mills, Farid, Selman, & Al-Hallaj, 2006), (Mills & Al-Hallaj, 2005) began exploring the use of an expanded graphite matrix that is impregnated with PCM to further increase the thermal conductivity of the wax. The performance of the plate was demonstrated by using it as a passive thermal management system for a battery module that was discharged at high rates. The results from the test was that the porous graphite matrix increased the thermal conductivity of the matrix by two orders of magnitude. The expanded graphite-PCM cold plate is now commercially available from All Cell Technologies, LLC.

The introduction of carbon into phase-change materials were being explored by multiple researchers looking to enhance the thermal properties. Elgafy and Lafdi (Elgafy & Lafdi, 2005) investigated the effects that carbon nanofiber additives had on the cooling rates during solidification. This sparked a large interest into the use of nano carbon strands and particles to be mixed with the PCM. The nano additives posed a good solution to issues seen with mixing in macro scale carbon fibers, but were considered a health risk due to inhalation. Regardless, the nano carbon strands did positively effect the thermal conductivity of the material to provide better cooling rates of the material. Additionally, investigations completed by Chintakrinda et al (Chintakrinda, Weinstein, & Fleischer, 2011), (Chintakrinda, Warzoha, & Weinstein, 2012) compared the use of the carbon nanofibers, expanded graphite, and aluminum

foams. It was determined that the graphite foam provided the best results for a PCM cold plate at higher heat fluxes without significant delay to steady state heat transfer, which provides valuable information for high power PCM cold plate designs.

### **2.3 The Push Into Electric Vehicles**

As the interest in electric vehicles grows larger, as does the need for more efficient batteries. Research by Park and Jung (Park & Jung, 2010) was looking into the cooling system architecture of series-hybrid electric vehicles. They looked at three independent designs that were each an active system, but had progressively less power draw. Of course, the system with the overall least amount of power draw proved more efficient in vehicle range, but not in cooling. They concluded that the use of a passive system in conjunction with a low power draw would prove to be efficient on both fronts.

Thus, the introduction of a passive thermal management system is imperative for maximizing electric vehicle range. The passive system has no additional power draw from the batteries and will keep the batteries at an optimal operating temperature, keeping the efficiency high. Studies conducted by Buford et al (Buford, Williams, & Simonini, 2011) investigated the most energy efficient cooling strategy for rechargeable energy storage systems, specifically for electric and hybrid electric vehicles. The research compared passive, active, and bypass systems using simulations and control strategies. Their work showed that the best option is a passive thermal management

system, but should include an active system for when the heat load is not being dissipated quickly enough.

### **2.3.1 Electric Vehicle PCM Implementation**

With the AllCell Technologies cold plate commercially available for implementation, investigators were studying its use with full-scale battery experiments. Work conducted by Kim et al (Kim, Gonder, Lustbader, & Pesaran, 2008) used a plate of the expanded graphite-PCM composite attached to an Aerovironment ABC-150 battery cycler to emulate battery conditions and expected heat loads during depletion. They repeated an aggressive drive cycle, known as the US06 drive cycle, to apply the highest loads to the PCM cold plate. The analysis suggested that the PCM is ideal for accepting large peak loads but that the overall battery management system should include an active cooling loop due to saturation of the plate.

The same AllCell Technologies cold plate was used by Sabbah et al (Sabbah, Kizilel, Selman, & Al-Hallaj, 2008) in the thermal management system of a Ford Escape Hybrid Vehicle. They discuss the PCM's ability to keep the battery pack below the safety limit of 55°C even under constant-rate discharge at rates as high as 10A per cell and high ambient temperatures of 45°C. The active system tested was incapable of recreating this result due to the higher ambient temperatures and was also pulling additional power from the batteries for the fans and pumps. Similar results can also be noted in the work done by Kizilel et al (Kizilel, Sabbah, Selman, & Al-Hallaj, 2009) who focused on the enhanced safety provided by the PCM from ther-

mal runaway and cell failure when compared to common air-cooled systems. Using the AllCell cold plate, the increased thermal conductivity from the graphite matrix allowed the heat to quickly and uniformly dissipate throughout the volume.

More recently, *EcoCAR 2: Plugging In To the Future*, Barsotti and Boetcher (Barsotti & Boetcher, 2013, (Barsotti & Boetcher, 2014)] implemented the AllCell Technologies cold plate, coupled with an active system, to the team's Chevrolet Malibu. Numerical simulations were also conducted and utilized the ideal properties and temperature melt ranges of the PCM cold plate. The data shows that the PCM cold plate and active cooling loop was effective in keeping energy consumption of the vehicle lower by limiting the active system pump usage. Additionally, the use of the PCM cold plate resulted in a more lightweight system resulting in even lower energy consumption than previously expected.



### 3. Phase-Change Material Modeling & Experimental Testing

To develop the PCM cold plate, experiments are conducted on a dedicated test bench to study the passive cooling system required to keep the battery modules below to the manufacturer's battery temperature maximum of 50°C. Once this is achieved, it will be possible to improve the charge-deplete (CD) range through the reduced usage of an active cooling system. Additionally, by keeping the battery modules at operating temperature the efficiency of the modules will increase during vehicle operation.

#### 3.1 Test Scope

In order to produce this result, a recent alternative to standard liquid-cooled cold plates, the PCM cold plate, will be investigated. Although PCM has many traits that allow this cold plate to be beneficial, the problem with the material is its naturally low thermal conductivity. This limits their ability as thermal management systems due to the difficulty in dispersing the heat throughout the full volume. Furthermore once it is saturated, it is also difficult to lose the waste heat stored within the PCM. A solution to this issue is to investigate the use of thermal conductivity enhancers to increase the overall thermal conductivity of the PCM. Common thermal conductivity enhancers include the use of a carbon or graphite based inclusion, such as Al Hallaj's expanded graphite (Al Hallaj & Selman, 2000) and Fukai's use of carbon fiber brushes

(Fukai et al., 2000), but metallic foams and shavings can also be used. Essentially any material with a higher thermal conductivity than the PCM can be added to the matrix and considered a thermal conductivity enhancer. In this study, loose carbon fibers will be added into the PCM in varying percentages by volume to determine the optimal mixture for increasing the thermal conductivity for managing the heat from the battery modules to the PCM.

### **3.2 Test Article**

The PCM to be used for these experiments will be PCM-37, which has an onset temperature of 34.5°C and a melt range of 5°C. This was selected in order to keep the battery modules below the manufacturer's battery temperature maximum of 50°C.

The PCM tray follows the design of a single battery module foot print. It is melted and poured into the aluminum tray, creating the cold plate. This cold plate is then encased in the aluminum tray support structure with a buna-n face seal installed to prevent leaks. The heat load is generated through a 40W Southeastern Thermal Systems silicon heater, which is powered from a variable voltage supply. The test sample is housed within DOW blue foam with a thermal resistance of 5 per inch which provides insulation to prevent heat flow out of the system. The test sample is instrumented with 8 type-E thermocouples that are monitored with an Agilent 34970A Data Acquisition System. The data is then sent for post processing onto a laboratory computer.

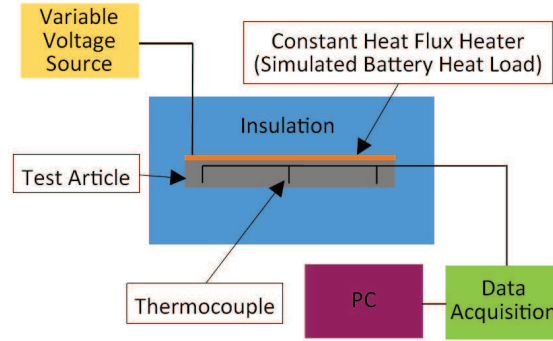


Figure 3.1.: Schematic diagram of the test bench setup.

The experimental setup follows the schematic diagram seen in Figure 3.1. The scenarios executed simulated the Joule heating from a single battery module into a PCM cold plate that match the footprint of the A123 battery module. The experiments were split into baseline experiments consisting of bulk PCM and an aluminum plate, and a parametric experiment with the 0 - 1% carbon fiber addition. A schematic of the PCM test sample can be seen in Figure 3.2.

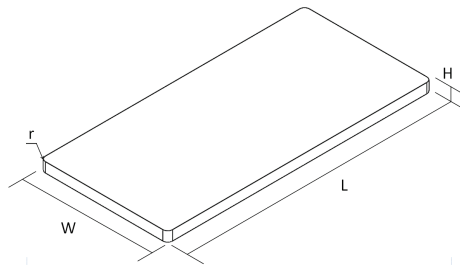


Figure 3.2.: Schematic of the PCM plate used for the experiment.

Table 3.1 shows the dimensions of the PCM cold plate used for the experimental setup.

Table 3.1.: Dimensions of the PCM test sample.

W	L	H	r
6.50 in	13.75 in	0.50 in	0.25 in
165.1 mm	349.25 mm	12.7 mm	6.35 in

The Southeastern Thermal Systems 40W heater was sized to match the  $600 \text{ W/m}^2$  nominal heat load over a  $0.057 \text{ m}^2$  area of a single module. This was adhered to an aluminum lid section that is designed to keep the a constant heat flux into the PCM cold plate. Figure 3.3 shows the aluminum lid piece that is bolted to an aluminum bottom tray.

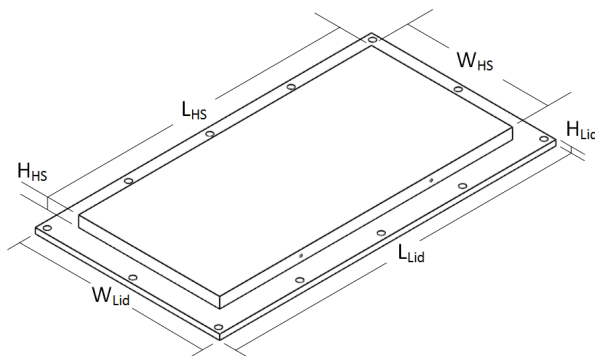


Figure 3.3.: Aluminum lid piece that is bolted to the aluminum bottom tray. The Southeastern Thermal Systems 40W heater is adhered to the top surface.

The PCM test piece is housed inside the bottom aluminum tray that is large enough to house the PCM tray with an adequate seal. The seal designed is a com-

Table 3.2.: Dimensions of the PCM top tray.

$W_{Lid}$	$L_{Lid}$	$H_{Lid}$	$W_{HS}$	$L_{HS}$	$H_{HS}$
8.50 in	15.5 in	0.25 in	6.5 in	13.75 in	0.75 in
215.9 mm	393.7 mm	6.35 mm	165.1 mm	349.25 mm	19.05 mm

pression face-seal created by a 0.25 in.-square-profile Buna-N seal. This was selected through a materials comparability study conducted with various seals. Buna-N was the only seal to survive repeated exposure to the PCM without quick degradation. Buna-N also provides a low cost and simple solution to the complicated sealing problem. The tray is also held together with the lid by 12, 1/4 - 28 bolts. The aluminum support tray and seal groove design of this test sample can be seen in Figure 3.4. This test piece is then put into 7 pieces of 2 inch Dow blue foam insulation with an R-value of 5 per inch.

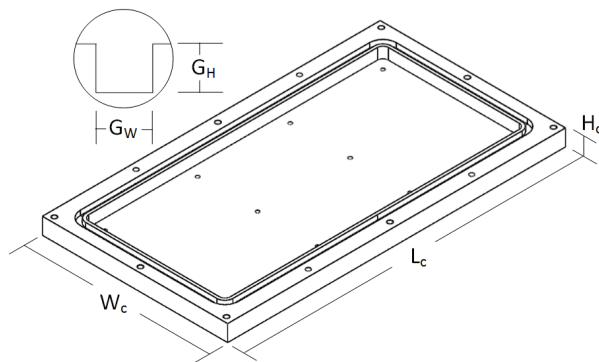


Figure 3.4.: Aluminum support tray and seal design of the PCM test sample.

Table 3.3.: Test container dimensions used for the experimental setup

W	L	H	$G_W$	$G_H$
8.50 in	15.5 in	0.75 in	0.25 in	0.21 in
215.9 mm	393.7 mm	19.05 mm	6.35 mm	5.33 mm

The outputs being monitored during experimentation are the temperatures of eight locations throughout the cold plate.

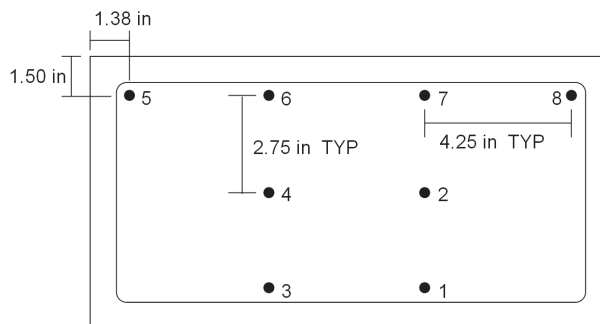


Figure 3.5.: Critical locations of the thermocouples used for the test bench experiment.

Figure 3.5 shows the critical instrumentation locations. These locations were selected due to the geometric symmetry and the expectation that they would provide the most information about the heating affects with the inclusion of the short loose carbon fiber.



Figure 3.6.: PCM test setup with thermocouples embedded in the plate.

The instrumentation used are type-E thermocouples to obtain the temperatures throughout the melt and solidification of the PCM. The type-E thermocouple was chosen due to the higher signal resolution ( $62 \frac{\mu V}{\%C}$ ) and accuracy over type-K and type-J thermocouples. The type-E thermocouples have been calibrated against the NIST traceable calibration thermometer. These measurements were then collected and recorded using the Agilent DAQ and were post processed on a laboratory computer. During the experiments, the temperature of the local environment was also recorded through a ninth type-E thermocouple to ensure a controlled experiment and evaluate the effect that higher ambient temperatures had on the melt profile exhibited by the PCM.

The test specimen is also assumed to have little to no air pockets within the matrix. This would create an insulation layer in the test piece, therefore affecting the time required to melt the PCM test sample. This assumption is also a major difference between the simulation used and the actual test bench setup. With the

simulation, the PCM plate was made isotropic which would not account for accidental inclusions, non-homogeneous mixing, and potential air pockets.

The limitations of the test setup include the assumption that the PCM volume is in perfect thermal contact with the heat source allowing the PCM to fully absorb the heat. With actual implementation, the PCM plate will not be in perfect thermal contact with heat source because there are multiple layers of metal enclosures with associated air gaps. The air gaps create a layer of insulation that keep the heat in the battery modules rather than allowing it to enter the PCM cold plate. This limitation will also be present in physical system installed on the vehicle, but is not included in the simulation.

### **3.3 Test Setup**

In order to complete the experiments a test bench was developed to simulate the Joule heating from the battery module into a PCM test sample. A schematic of the system setup is seen in Figure 3.7.

The batteries selected for vehicle implementation are the A123 AMP20 15S3P battery modules. These battery modules consist of 18 individual lithium-ion cells. The vehicle has seven of these modules to make up the energy-storage system (ESS). To properly model the heat generation from the ESS, the complete Emissions & Energy Consumption (E&EC) drive cycle data obtained from EcoCAR 2 competition is used. The heat flux over the drive cycle can be seen in Figure 3.8.



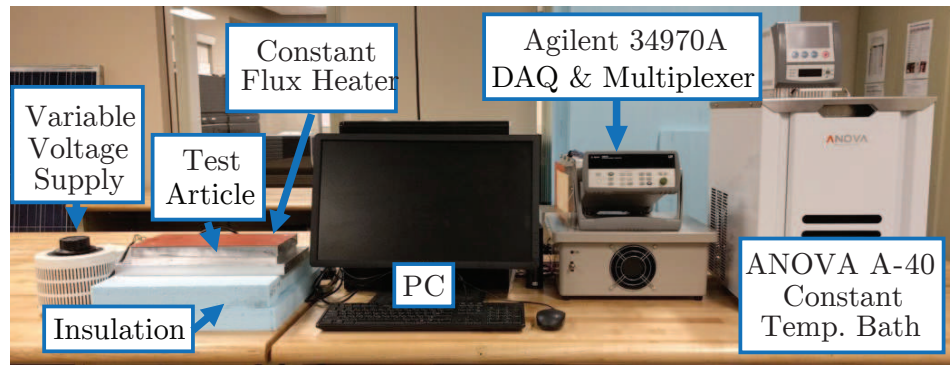


Figure 3.7.: Image of the test bench setup with critical components.

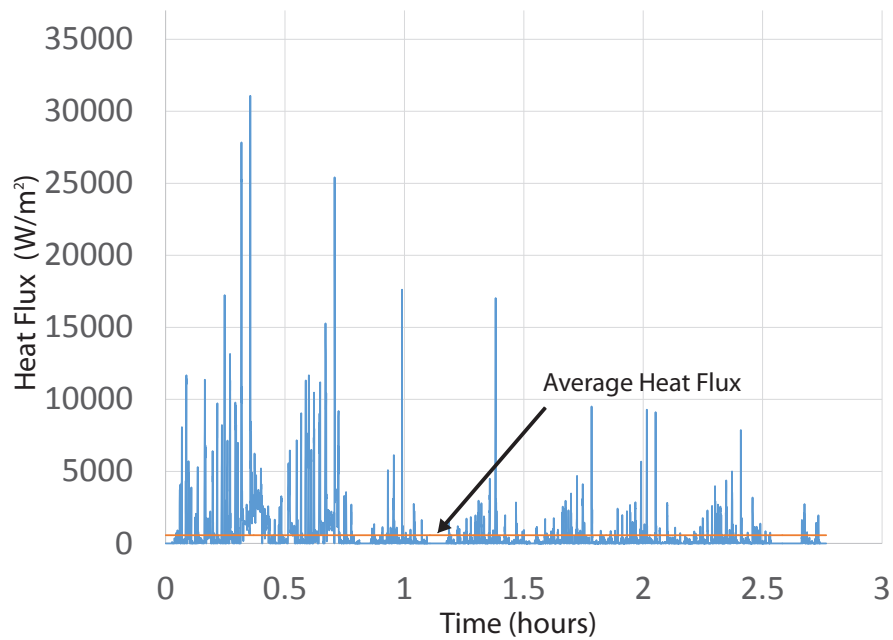


Figure 3.8.: Heat flux values over the complete E&EC drive cycles of the EcoCAR 2 competition.

The heat load varies with time due to the higher thermal loads during CD mode. Since the thermal energy produced through chemical reactions is minimal, the heat

flux will only be determined off of the internal resistance and current draw of the battery module. Heat flux is derived using the following equation:

$$q'' = \frac{I^2 R}{A_c} \quad (3.1)$$

In Eq. 3.1,  $q''$  is the heat flux,  $I$  is the current draw,  $R$  is the internal resistance of the battery module, and  $A_c$  is the contact area of the module.

From Equation 3.1 and previous E&EC data, an average heat flux of  $570 \frac{W}{m^2}$  is calculated. This was rounded to  $600 \frac{W}{m^2}$  for testing through the available off-the-shelf heaters. Although this value is from EcoCAR 2, the data from the 2013 Chevrolet Malibu is applicable to the 2016 Chevrolet Camaro due to the similarities in vehicle mass and characteristics.

In addition to the test bench setup, thermal characterization equipment is used to determine important thermal properties of the carbon fiber and PCM matrix. A Guarded Hot Plate will be used to determine thermal conductivity ( $k$ ) and a Mettler Toledo DSC 3 Differential Scanning Calorimeter will be used to determine the specific heat ( $C_P$ ), latent heat of fusion ( $h_{sl}$ ), and onset melting point ( $^{\circ}C$ ) of our matrix.

### 3.4 ANSYS Modeling

A numerical solution in ANSYS APDL was conducted on the bulk PCM-37. The ANSYS APDL model consisted of a 1D model that is one element wide with 100 structured cells down the 12.7 mm (0.5 in) thick PCM plate. Figure 3.9 shows the model used for the ANSYS APDL simulation.

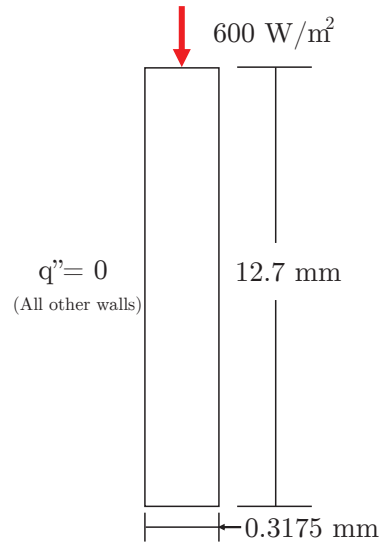


Figure 3.9.: ANSYS APDL model used for the preliminary simulation

In order to simulate the melt of the phase-change material, the enthalpy method defined by Shamsunder and Sparrow [(Shamsundar & Sparrow, 1975)] is used. This method solves the conservation of energy equation below:

$$\frac{\partial h}{\partial t} = k \left[ \frac{\partial^2 T}{\partial x^2} + \frac{\partial^2 T}{\partial y^2} + \frac{\partial^2 T}{\partial z^2} \right] \quad (3.2)$$

In Eq. 3.2,  $h$  is the enthalpy,  $t$  is the time,  $k$  is thermal conductivity,  $T$  is the temperature, and  $x$ ,  $y$ , and  $z$  are the coordinates. The enthalpy per unit mass as a function of temperature is shown in Table 3.4. These enthalpy values were calculated using a datum of 1 °C for the temperature.

Table 3.5 shows the material properties from a manufacturer's data sheet of the PCM input into ANSYS APDL. The heat flux boundary condition of  $600 \frac{W}{m^2}$  was applied to the top face of the model.

Table 3.4.: Enthalpy values calculated for use in the enthalpy method simulation.

Temperature [ $^{\circ}\text{C}$ ]	Enthalpy [ $\frac{\text{J}}{\text{kg}}$ ]
1	0
35.4	68,482
39.5	239,653
300	772,180

Table 3.5.: Material properties of the PCM utilized for numerical modeling.

Property	Value
Density $\rho$ [ $\frac{\text{kg}}{\text{m}^3}$ ]	925
Thermal Conductivity $k$ [ $\frac{\text{W}}{\text{m}\cdot\text{K}}$ ]	0.25
Latent Heat of Fusion $h_{sl}$ [ $\frac{\text{J}}{\text{kg}}$ ]	174,000
Melt Onset [ $^{\circ}\text{C}$ ]	34.5
Melt Range [ $\Delta^{\circ}\text{C}$ ]	5

The remaining walls were given adiabatic boundary conditions. This was taken as a worst case scenario by causing all of the heat energy to be absorbed into the PCM.

A mesh independence study was conducted using 200 structured cells.  $T_{Probe}$  was taken at the left corner of the bottom element and was compared between the two simulations. A maximum variance of 0.77% was seen between the two simulations.

An additional preliminary thermal conductivity analysis was conducted using the same model in ANSYS APDL. The investigation observed the effect of varying the thermal conductivity of the PCM. The data is used to determine the ideal matrix of carbon fiber and PCM by predicting thermal conductivity target for the experimental tests. Figure 3.10 shows the difference in melt characteristics of the PCM once the thermal conductivity has been shifted.

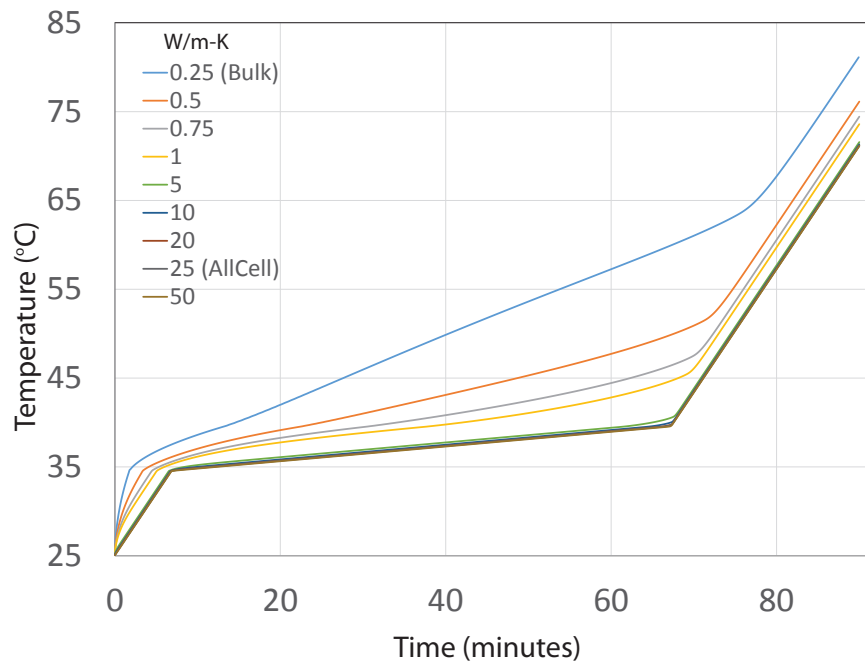


Figure 3.10.: ANSYS APDL simulation data of bulk PCM-37 to observe the difference in melt characteristics by varying thermal conductivity.

The simulation was used to determine the target thermal conductivity, not to determine actual performance characteristics of the PCM as a thermal management system. To execute this, the simulation only needed to be a one dimensional and

fully adiabatic model. These conditions are unable to be replicated experimentally. In addition to this the material models were given from Pure Temp, which in previous work has been identified as being inaccurate.

#### 4. Discussion of Results

The baseline experiments were conducted first in order to obtain controls for the parametric experiments. The primary baseline experiments consisted of the PCM-37 and a sample of PCM-48. This experiment was to select the PCM that would keep the battery modules below the battery manufacturer's specifications of 50°C. Figure 4.1 shows the temperature versus time data for thermocouple 2 observed during the bulk 37 and 48 melt experiments. Thermocouple 2 is selected due to its location being near the center of the plate. The melt of the PCM-37 and PCM-48 begin at approximately 34°C and 45°C, respectively. During the plateau region, the PCM is melting at constant temperature until it spikes. This spike is when the PCM is completely saturated and is now beginning to degrade. It is seen that the PCM-37 takes approximately 2.75 hours to reach the manufacturer's specification. Although, the PCM-48 stays under 50°C longer, the PCM-37 keeps the battery cooler overall resulting in a more efficient discharge from the battery module.

As an additional baseline experiment, the aluminum plate experiment was conducted to compare the bulk PCM to a standard aluminum cold plate design. The temperature versus time data from thermocouple 2 for the aluminum test sample is shown in Figure 4.2. The aluminum cold plate is seen to have linear heating properties. This is due to being a homogeneous material with constant thermal properties.

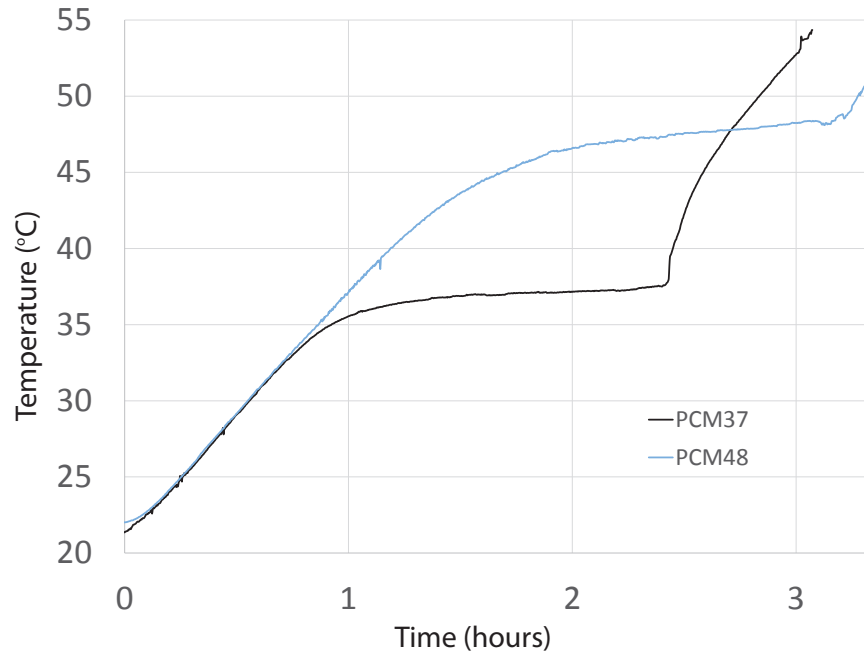


Figure 4.1.: Heating and melt data observed during the bulk 37 and 48 experiments for thermocouple 2.

This data shows that it takes just over 1.5 hours to reach the manufacturer's specification, indicating that the aluminum cold plate is not ideal for longer vehicle drive cycles. The aluminum cold plate is also incapable of handling large power spikes from the battery modules, and would require a large active cooling system to remove the waste heat.

The parametric experiments consisted of four variations of the carbon fiber PCM matrix. The temperature versus time graph of thermocouple 2 for various concentrations of carbon fiber can be seen in Figure 4.3. The results of these experiments show that with the current test setup, the 0.5% will provide the best results in heating and



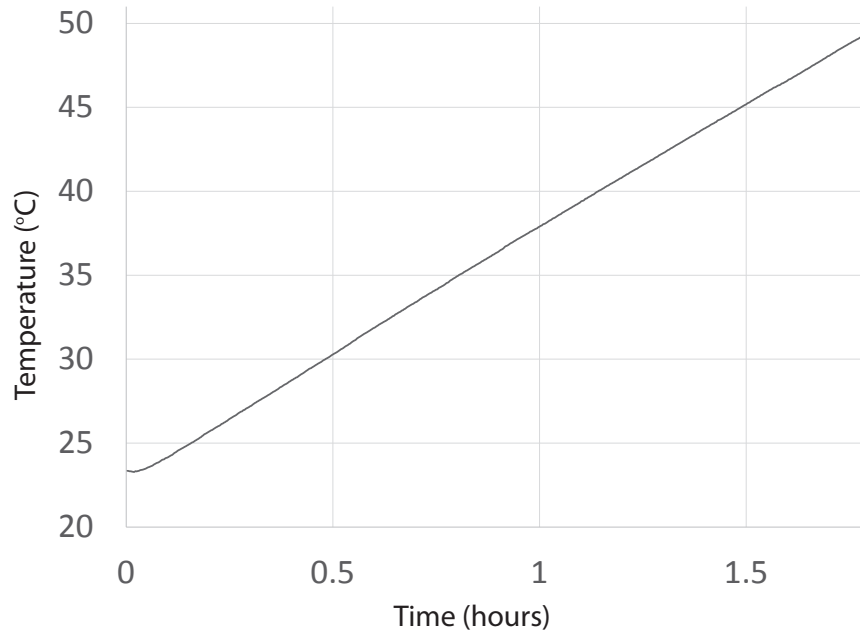


Figure 4.2.: Heating data of the aluminum baseline experiment.

melting properties. At the end of the melt, the 0.5% is shown to steadily increase in temperature instead of experiencing a sudden spike similar to the bulk PCM. The 1% and 0.25% appear to decrease the melt time of the PCM-37 by up to a 0.5 hours and the 10% by 1 hour. By comparing the 1% data to the 10% data, it can be suggested that the 1% may also be a good choice for the maximum addition since it is also drastically affecting the melt time of the PCM. This can either be attributed to the decrease in thermal storage capacity caused by the introduction of the carbon, or the increase in thermal conductivity that is being investigated.

The initial test of 10% demonstrated that the inclusion of a high volume ratio of carbon to PCM affects the melt characteristics of the PCM. It was observed that

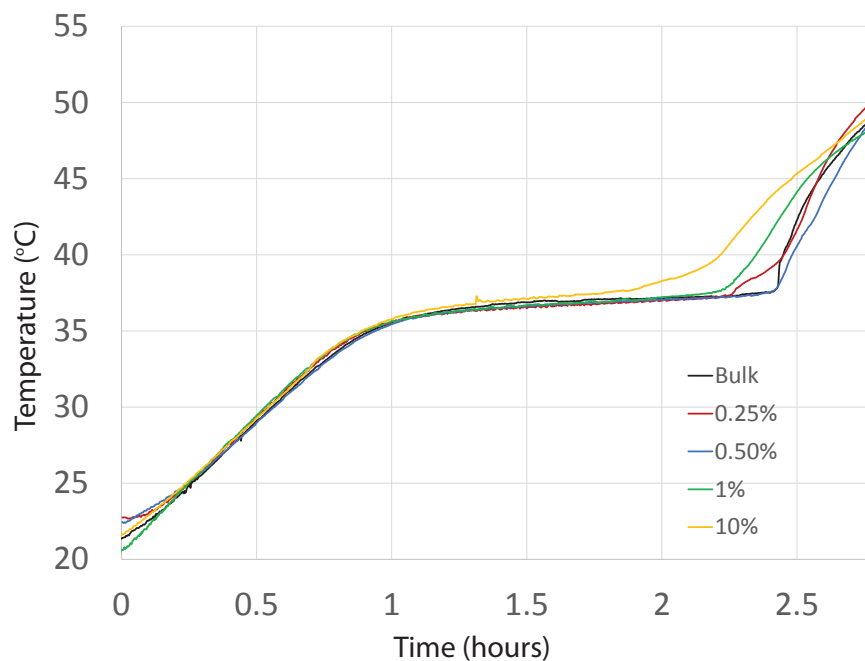


Figure 4.3.: Temperature versus time of thermocouple 2 data for each of the parametric experiments compared to bulk PCM-37.

the high volume ratio resulted in an uneven surface, creating air pockets when the test sample is heated. Figure 4.4 shows the uneven surface created through the PCM resolidifying unevenly.

These air pockets can affect the PCM's ability to melt properly by creating an insulation layer between the top surface and heat source. Thus experiments with smaller volume ratios were completed. It was discovered that the smaller ratios did not affect the surface texture. This can be seen in the solidified sample of the 1% sample in Figure 4.5. Therefore, the experiments were modified to be between 0 - 1 % in carbon additions.

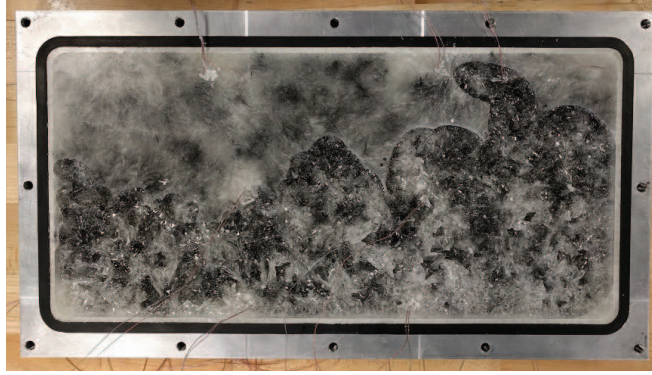


Figure 4.4.: Uneven surface of the 10% sample that was created due to uneven solidification of the PCM.

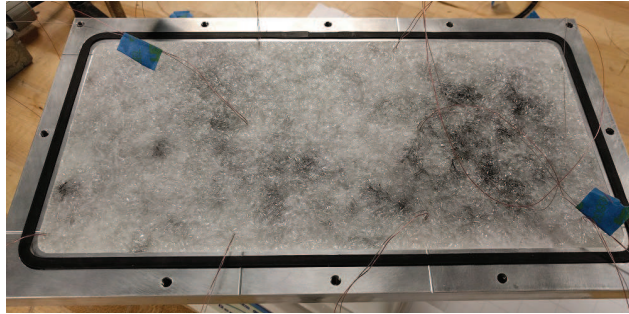


Figure 4.5.: The surface of the 1% test sample. Note that it is smooth and without any air pockets.

The comparison between the numerical and experimental data is shown in Figure 4.6. As expected, the numerical model is not accurate to the physical test. The numerical model completes the melt 1.5 hours faster and is  $27^{\circ}\text{C}$  warmer at full saturation when compared to the thermocouple 2 data from the 1% experiment data curve. This can be attributed to the assumption that the model is 1D with adiabatic walls.

The heat in the physical experiment will eventually exit through the boundaries and enter the aluminum structure, which the model is currently incapable of showing. Furthermore, the numerical model cannot recreate the PCM properties accurately. The thermal properties input in the numerical model are what the manufacture provides, which may not be enough to accurately depict the melt of the PCM.

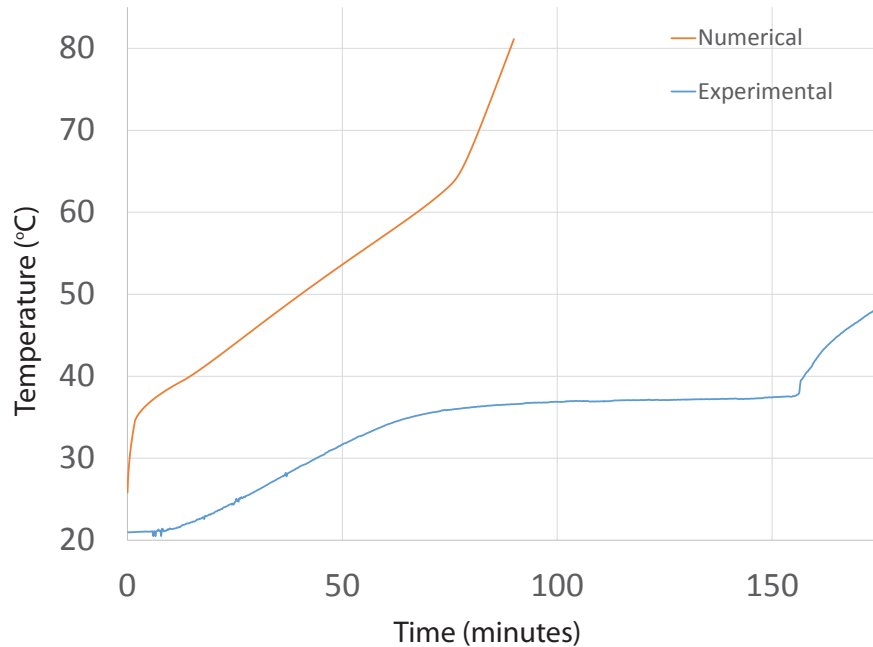


Figure 4.6.: Temperature versus time curve of the numerical and experimental comparison.

However using the experimental data, a more suitable model can be developed using the thermal properties of the modified carbon fiber PCM matrix. By using the PCM thermal properties obtained from the research, a more accurate battery thermal management system can be created in the overall EcoCAR 3 vehicle Simulink plant

model. This will be done through a lookup table from the experimental data that provide the melt characteristics of the PCM as a function of temperature provided from the battery modules. This will provide a more accurate approach on the ESS thermal management design and cooling system requirements. To obtain the necessary thermal properties, a test sample will be characterized thermally utilizing laboratory equipment such as the Mettler Toledo DSC 3 Differential Scanning Calorimeter and the ASTM Guarded Hot Plate Test.

Research conducted by Fukai et al.(Fukai et al., 2000), shows similar melt curve data for phase-change materials. Although the melt times are different between the two studies, the melt trends are the same, which indicates that the PCM used for the experiments are behaving as expected and melting at their intended melt onset temperature of 34.5°C.

Additionally, more experiments will be conducted in order to obtain a more refined carbon fiber to PCM volume ratio. Once the thermal conductivity can be obtained from the ASTM Guarded Hot Plate Test, more rigorous testing can occur to reach the target thermal conductivity increase while maintaining a suitable carbon fiber to PCM volume ratio.

## 5. Guarded Hot Plate Apparatus

Once the cold plate has been developed and tested experimentally, it can be characterized in order to determine its thermal properties. The desired affect from the testing is to observe an increase in thermal conductivity. As stated, the low thermal conductivity of PCM limits its ability as a thermal management system since the heat cannot disperse easily and evenly throughout the cold plate volume. But to test for thermal conductivity, an additional test instrument must be developed. This test bench will follow the design guidelines of the test apparatus designed by A. Mills et al and the ASTM specification for the Guarded Hot Plate Test. Mills et al (Mills et al., 2006) have developed a simple test setup in order to determine the thermal conductivity of their PCM sample and the ASTM C177-13 (ASTM International, ASTM C177-13) discusses the development considerations for creating a Guarded Hot Plate Apparatus. Figure 5.1 shows the basic schematic of the test setup to be developed.

The guarded hot plate apparatus utilizes a hot and cold plate that are held at a constant surface temperature. The known sample and the test sample sandwiched between the plates. Having the known sample, in this case stainless steel, allows the problem to be solved due to the heat flux through the sample to be calculated from the known thermal properties. The sample sizes can range between 0.50 and 1 meter in length or diameter. The large specimen size allows the end effects of the cold and

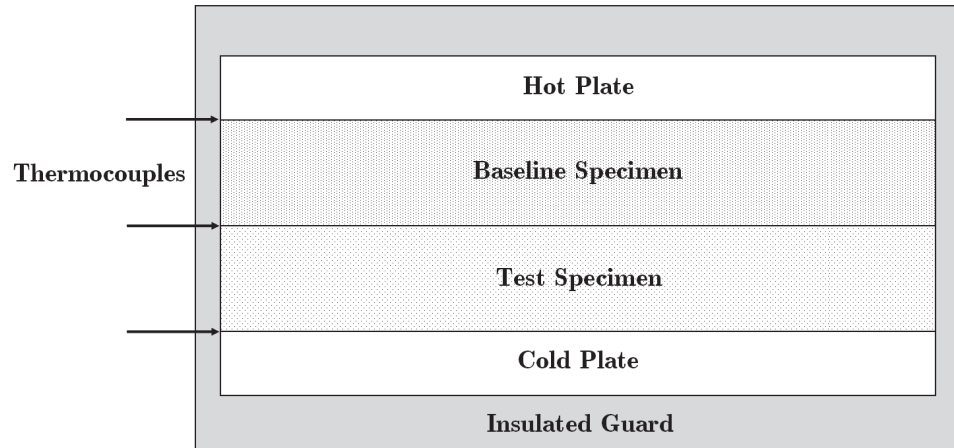


Figure 5.1.: Diagram of guarded hot plate test apparatus.

hot plates to be ignored since all that is needed is an isothermal region on the plate surface. To limit the heat loss with the environment, an adiabatic guard surrounds the samples and plates. Minimizing the heat loss to the surroundings will ensure that the heat flow through the plates and samples will be one-dimensional. Following Figure 5.1, thermocouples are used to obtain temperature data between the plates and samples. This can be done with multiple thermocouples or as little as three at the center of the plates. Once temperature data is obtained, Fouriers Law of Heat Conduction can be used to calculate the thermal conductivity and the test specimen can be thermally characterized. Fouriers Law or the Law of Heat Conduction, is the relationship between the rate of conduction in a material and temperature gradient in the direction of heat flow.

$$q'' = -k \frac{dT}{dx} \quad (5.1)$$

In this equation,  $q''$  is the heat flux,  $k$  is the thermal conductivity,  $T$  is temperature, and  $x$  is the distance along the direction of heat flow. It is important to note that this equation only works with one-dimensional heat transfer applications.

Before the tests can be completed, the Guarded Hot Plate Apparatus must be developed. The Guarded Hot Plate requires an isothermal boundary condition, or constant surface temperature, on the hot and cold plates. To do this a cold and hot fluid will flow through tubing attached to the plates. To create the most optimal cold and hot plates, the plate thicknesses, heat exchanger tube locations and, geometry will be investigated. The hot and cold plates shall have the interfaces be isothermal with a maximum temperature gradient of  $0.1^{\circ}\text{C}$  while minimizing material usage to keep costs low. Additionally, the parameters shall guarantee one-dimensional heat conduction through the plates and into the samples. It is important to ensure a one-dimensional heat conduction in order to maintain Fourier's Law of Heat Conduction for the system. The easiest way to force this condition is to increase the surface area and thickness of the plates. The increased area and thickness allow for the end effects of the insulated plates to be ignored while having an isothermal boundary condition that is one-dimensional within the remaining large plate area.

There are two simulations to be completed using the selected parameters; heat conduction and computational fluid dynamics (CFD). These simulations will be used to determine the optimal configuration of the parameters in order to satisfy the isother-



mal interfaces and one-dimensional heat conduction requirements of the plate design. The data from these simulations will also be used for validation when the full test apparatus is assembled.

## 5.1 Plate and Tubing Design

The hot and cold plate designs will both act as a simple heat exchanger where a fluid of a specified temperature will be pumped through tubing that is in thermal contact with the plates. The design shown in Figure 5.2 follows Mills et al (Mills et al., 2006) utilizing a hot plate on top with constant temperature fluid flowing through each of the tube sections.

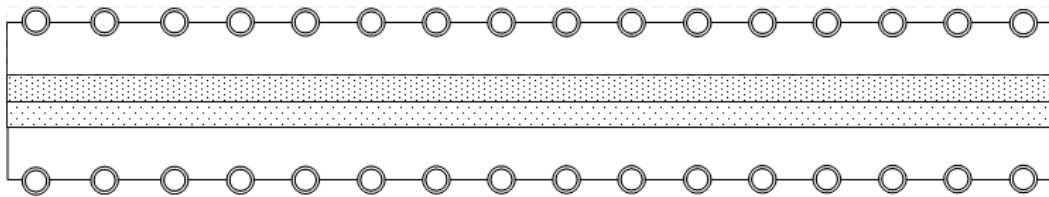


Figure 5.2.: Initial tube and plate design.

### 5.1.1 Solution Domain

A parametric study focused on the plate thickness and number of tube loops to ensure the isothermal boundary condition required. The diameter of the tubes are to be fixed at 12.7 mm (0.50 in). Figure 5.3 shows the two design variables with

the assembly. The thickness and number of tubes will be the most important factors when creating the one-dimensional heat transfer.

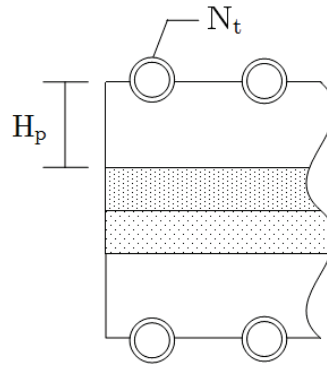


Figure 5.3.: Variables to be studied during experiments.

Two-dimensional simulations were used for the cases since the geometry of the design was the focus. The three-dimensional effects on the system are not important until the number of tubes and plate thickness can be finalized. Furthermore, the two-dimensional case allows the model to be simplified to decrease computation time for the parametric studies. In order to determine the best configuration of parameters, 5 cases were observed. Each case utilized either a 12.7 mm (0.50 in) or 25.4 mm (1.0 in) thick aluminum plate with 4–12 tubes used in each plate. Table 5.1 shows the test cases explored in the two-dimensional simulations.

Table 5.1.: Investigated cases for parametric study

Parameter	Case 1	Case 2	Case 3	Case 4	Case 5
Plate Height ( $H_p$ ) [mm]	12.7	12.7	12.7	25.4	25.4
Number of Tubes ( $N_t$ )	4	8	12	8	12

### 5.1.2 Governing Equations, Boundary Conditions, and Initial Conditions

The two-dimensional unsteady heat conduction equation, Eq. (5.2), is solved in the simulations.

$$k \left( \frac{\partial^2 T}{\partial x^2} + \frac{\partial^2 T}{\partial y^2} \right) = \rho C_p \frac{\partial T}{\partial t} \quad (5.2)$$

In the preceding equation,  $x$  and  $y$  are the Cartesian coordinates.  $T$  is temperature and  $t$  is time. The material properties are  $k$  is the thermal conductivity,  $\rho$  is the density and  $C_p$  is the specific heat capacity. Material properties for the solids used were obtained from Matweb and are shown in Table 5.2. High Density Poly-Ethylene (HDPE) was selected as the PCM replacement for the simulations due to the similarities in material properties without including any solid to liquid phase transition in the model.

To properly model the heat conduction through the test specimens, the boundary conditions for the model must be set. Figure 5.4 shows the boundary and initial conditions set for the model. The model was cut in half at 508 mm (10 in) due to symmetry and will help lower computational requirements. Thus, the right wall has the symmetry boundary applied. The inside of the top set of tubes are given an

Table 5.2.: Material Properties of HDPE and 304 Stainless Steel used for simulations.

Material	HDPE	304 Stainless Steel	Aluminum
Density $\rho$ [ $\frac{kg}{m^3}$ ]	947	8,000	2,719
Thermal Conductivity $k$ [ $\frac{W}{m.K}$ ]	0.49	16.2	202.4
Specific Heat, $C_p$ [ $\frac{kJ}{kg.K}$ ]	2,500	500	871

isothermal wall condition with a temperature of 318.15K and the lower tubes were given the same condition with a temperature of 281.15K. All remaining boundaries of the assembly have an adiabatic condition applied.

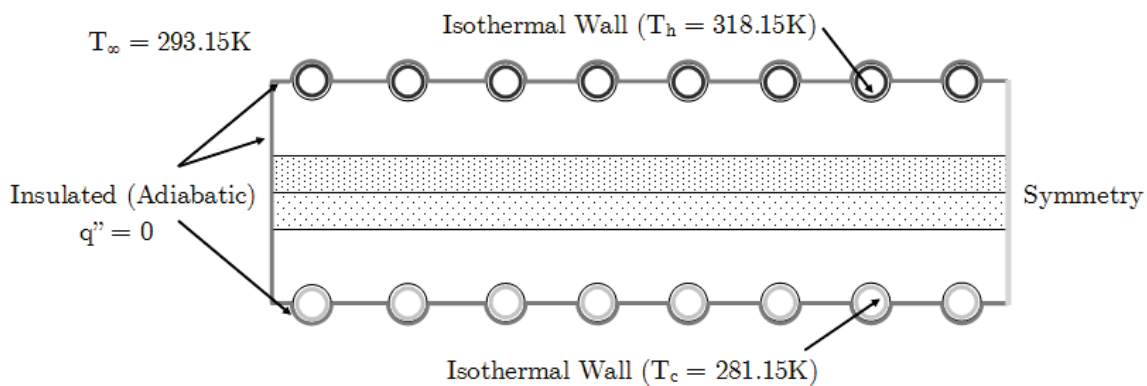


Figure 5.4.: 2D simulation boundary and initial conditions.

### 5.1.3 Solution Details

The parametric studies were simulated using ANSYS Fluent 16.0. This software is a commercially available finite volume based solver. The mesh for each simulation was created in Pointwise 17.3R5. The mesh for each case utilized a node spacing of 1.27 mm (0.50 in) of unstructured tetrahedral cells that varied between 24,000 for 12.7 mm (0.50 in) thick plates, and 37,500 elements for the 25.4 mm (1.0 in) thick plates. Figure 5.5 shows the mesh sizing used for Case 4, but the mesh sizing for each other case is similar. A mesh independent study was conducted on Case 3 and Case 4 with 98,000 and 153,000 cells, respectively. Surface temperatures were compared between the hot and cold plates of each case and a maximum variance of less than 0.1% was seen in the study.

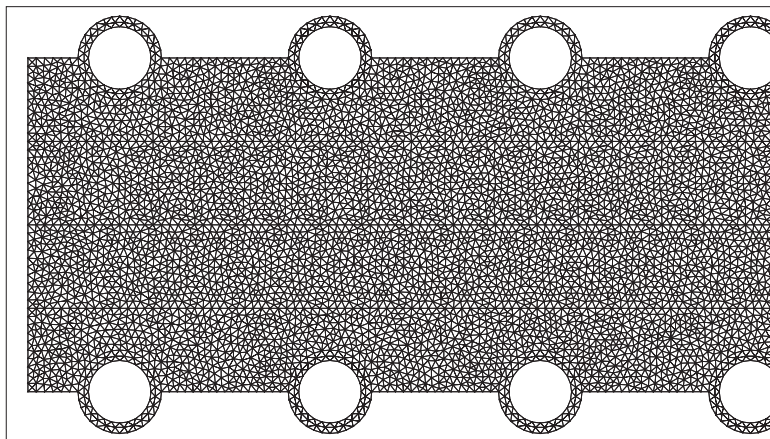


Figure 5.5.: Mesh used for the 2D simulations.

Since the final temperature profile of the plate is the focus of the study, the cases were considered steady and run for 5,000 iterations. This allowed the run to fully

converge with energy residuals as low as  $1^{-16}$  showing no change was observed with any additional iterations.

#### **5.1.4 Results**

The parametric study was used in order to obtain the optimal design of the cold and hot plates. This included five cases of varying the number of tubes and the plate thickness. These variables have the highest impact for ensuring that the plate has one-dimensional heat transfer with an isothermal boundary condition on the contact surface. A comparison of the five cases in the study was conducted in order to determine the optimal design to create the required parameters.

##### **5.1.4.1 Case 1**

The initial case investigated used four tubes spaced evenly through a 12.7mm (0.5in) thick aluminum plate. Figure 5.6 shows the temperature contour through the assembly. It can be seen that the temperature differential occurs within the HDPE sample indicating that this design will allow us to determine the thermal conductivity of the test sample. Since this effect is seen in the four tube case, it is expected to be true for each proceeding case. However in order to validate the design, the cold and hot plates will be observed separately to see the temperature variance across their surfaces.

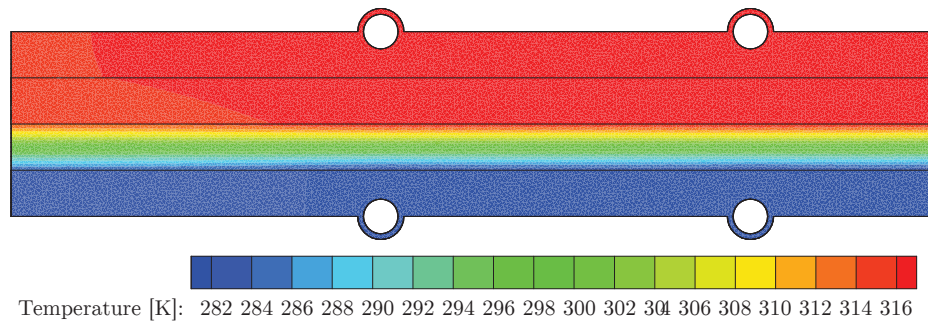


Figure 5.6.: Temperature contour seen for Case 1.

Upon investigation of the cold and hot plates it is determined that the four tube design does not provide sufficient cooling and heating to the surface. The temperature contours of the plates can be seen in figures 5.7 and 5.8. Note that the end effects of the plates, with up to 2K of variance, can be neglected due to the large surface area of the plate.

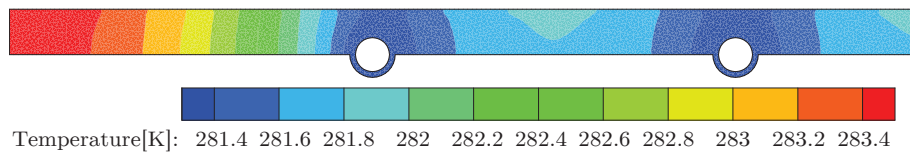


Figure 5.7.: Temperature contour for the cold plate of Case 1.

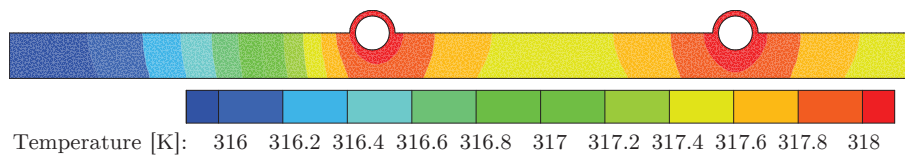


Figure 5.8.: Temperature contour for the hot plate of Case 1.

Looking at the surface temperature specifically, a large maximum temperature change of 0.25K between the tube locations can be seen in figure 5.9. This large temperature gradient is indicative of not having enough cooling and heating bodies within the assembly. In order to mitigate this, more tubes must be applied to the plates.

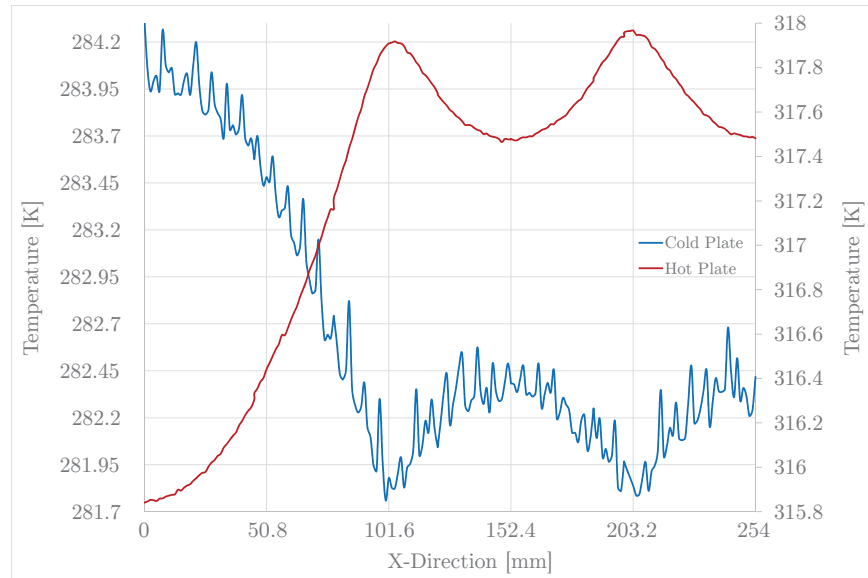


Figure 5.9.: Plot of surface temperatures observed for Case 1.

#### 5.1.4.2 Case 2

Since the four tube design did not provide enough heat transfer, the second case of the study will use eight tubes going through the 12.7mm (0.5in) aluminum plate. The temperature contour can be seen for this case in figure 5.10. As expected, the temperature differential is located within the HDPE sample. Like the previous case,



each plate must be inspected individually to see if adequate heat transfer is achieved through this design.

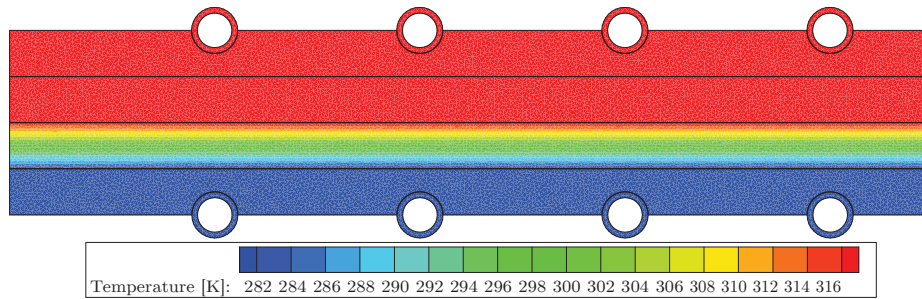


Figure 5.10.: Temperature contour seen for Case 2.

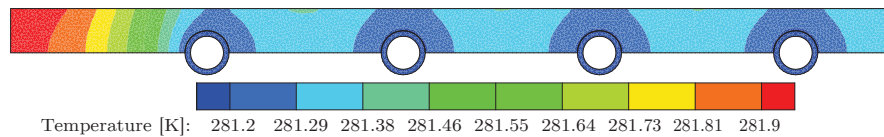


Figure 5.11.: Temperature contour for the cold plate of Case 2.

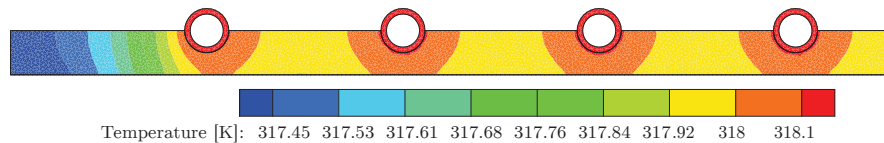


Figure 5.12.: Temperature contour for the hot plate of Case 2.

The cold and hot plate temperature contours are shown in figures 5.11 and 5.12. The temperatures of these plates are spread much more evenly through the plate, however, a maximum temperature differential of 1.25K is seen in figure 5.13. From the temperature contours it can be seen that the area around the tubing is being

affected, but there is still not enough tubing to change the temperature of the entire plate. Similarly to the first case, since the eight tube design did not adequately create the isothermal boundary needed, more tubing will be added.

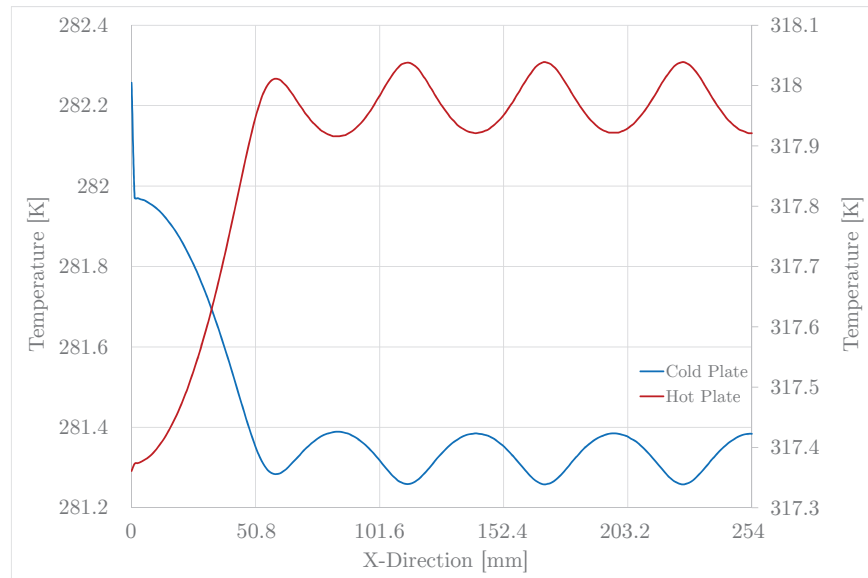


Figure 5.13.: Plot of surface temperatures observed for Case 2.

#### 5.1.4.3 Case 3

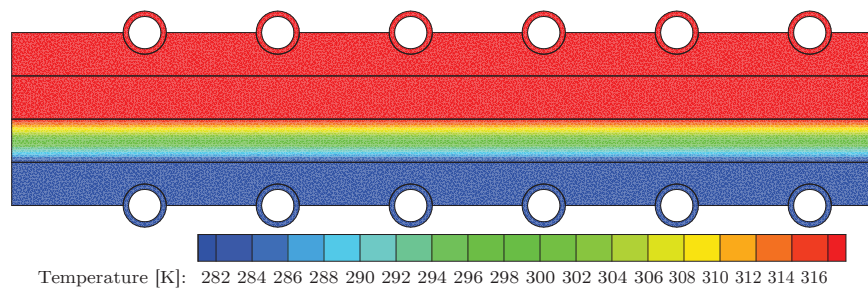


Figure 5.14.: Temperature contour seen for Case 3.

Case 3 of the study uses twelve tubes to go through the 12.7mm thick aluminum plate. Figure 5.14 shows that with the addition of four more tubes, the temperature drop is minimal. As before, investigation of the cold and hot plates independently yield that the 12 tube configuration satisfies each requirement. Figures 5.15 and 5.16 show how the additional tubes create a more constant contour across the surface than the previous cases.

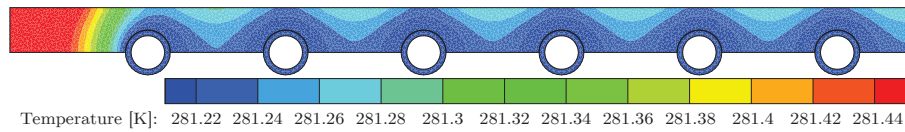


Figure 5.15.: Temperature contour observed for the cold plate of Case 3.

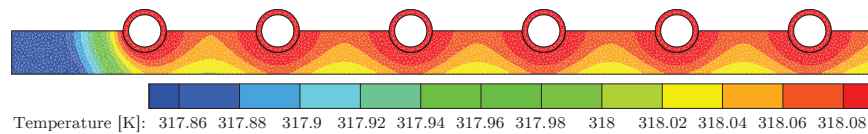


Figure 5.16.: Temperature contour observed for the hot plate of Case 3.

The plot in figure 5.17 shows that across the surface, over 406mm (16in) will be within 0.05K providing the isothermal boundary condition needed for the assembly. Therefore, twelve tubes will be used for the cold and hot plate designs.

#### 5.1.4.4 Case 4

Although the twelve tube in the 12.7mm plate satisfies the requirements, additional simulations on the plate thickness are to be done. In the previous cases, the

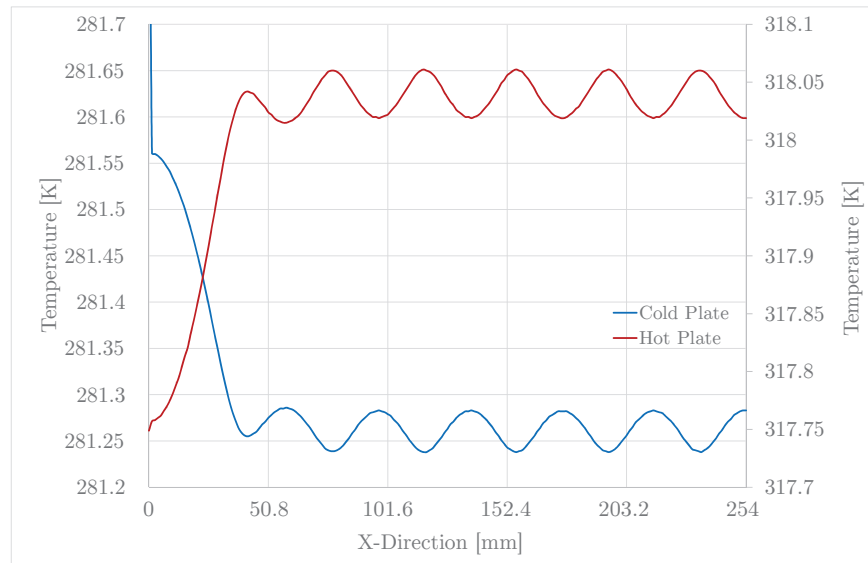


Figure 5.17.: Plot of surface temperatures observed for Case 3.

12.7mm plate showed that the cooling and heating from the tubing, although within the requirements for the isothermal surface, resulted in larger temperature differentials within the plate volume. This could cause issues with the flow being two-dimensional rather than the one-dimensional heat flow that is needed for Fourier's Law. By increasing the thickness, the heat will spread more evenly through the plate and the heat transfer can be assumed one-dimensional.

Case 4 examines the eight tube design with a 25.7mm (1.0in) plate since the results from Case 2 were close to the requirements. With the increased thickness, the impact from the tubing should be limited giving the heat flow enough distance to become one-dimensional and isothermal.

Since the assembly contour was good from Case 3, the plate contours will only be investigated. Figures 5.18 and 5.19 show the temperature contours seen with the

increased plate thickness. The contour bands from the tubing are evened out as they reach the bottom surface resulting in a more uniform temperature across it. This will provide a better isothermal boundary and ensure that there is one-dimensional heat flow into the stainless steel sample. This design also fulfills the major requirements of having a temperature differential of 0.1K or less with a maximum temperature variance of just over 0.08K across the surface.

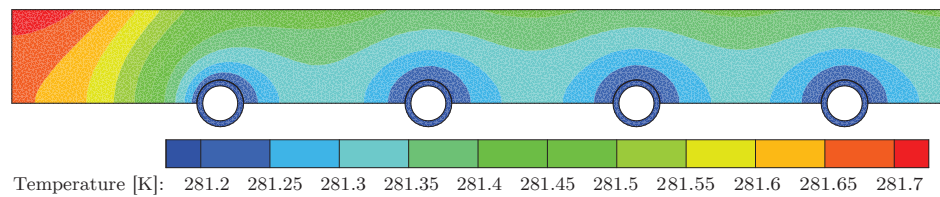


Figure 5.18.: Temperature contour of the cold plate for Case 4.

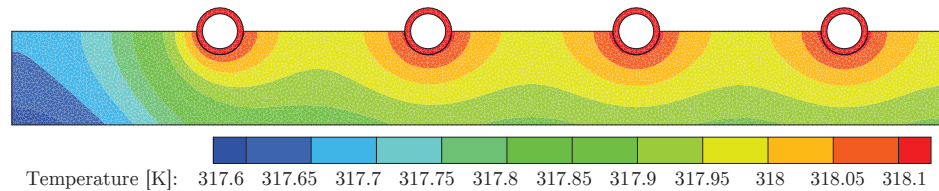


Figure 5.19.: Temperature contour of the hot plate for Case 4.

#### 5.1.4.5 Case 5

Case 5 takes the previous case a step further to see if the temperature variance can be dropped even further. The study will use twelve tubes embedded into a 25.4mm (1.0in) aluminum plate. As with the eight tube case, it is expected that the plate

thickness increase will cause the heat flow to become one-dimensional. With the added tubes, the temperature should also be fairly constant along the surface.

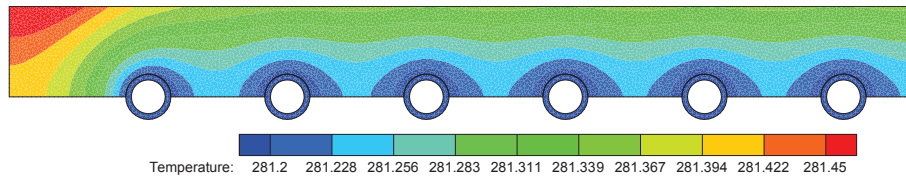


Figure 5.20.: Temperature contour of the cold plate for Case 5.

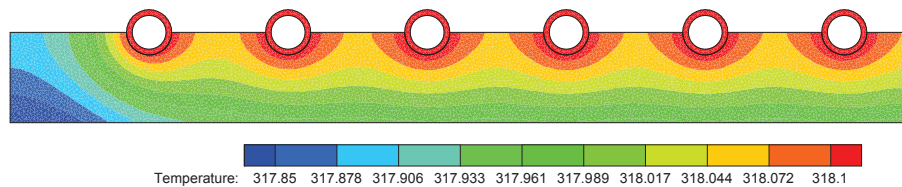


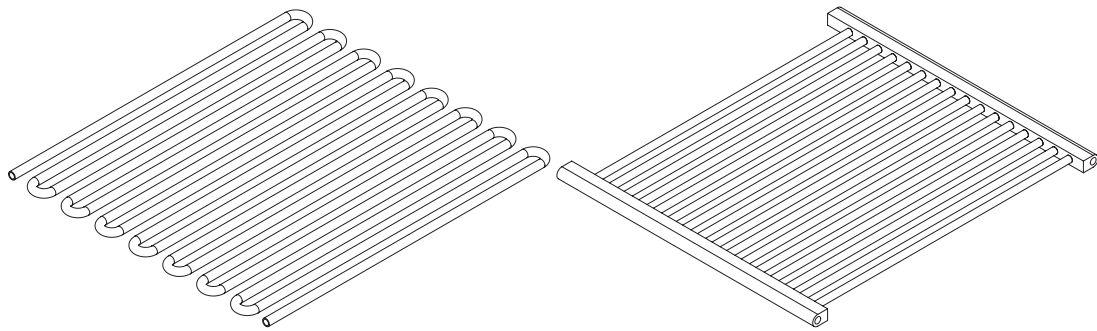
Figure 5.21.: Temperature contour of the hot plate for Case 5.

With this setup a temperature variance across the surface of the plates of less than 0.05K is seen. However, since minimal material is also needed for the setup, the twelve tube design adds more complexity and cost to the assembly when the eight tube design fulfills each requirement. Therefore, Case 4 will be used for the three-dimensional case in order to check the pressure and heat transfer effects with the fluid flowing through the tubing.

## 5.2 Tube Configuration Study Using ANSYS CFX

The cases above were used to find the optimal plate and tube design to ensure that the surface temperature was isothermal and had one-dimensional heat flow.

The tubing profile must be designed in order to retain that isothermal surface. This simulation will require a three-dimensional case with fluid flow through the pipe. The designs to be investigated are a single serpentine type heat exchanger tube design and a tubing manifold with the eight tube design from Case 4, however, the serpentine is preferred. If the serpentine tube is successful in fulfilling the requirements, the manifold will not be studied. In figures 5.22a and 5.22b, the two tubing designs can be seen; a serpentine heat exchanger tube and a designed manifold.



(a) Single serpentine tube design

(b) Manifold design.

The first tubing design utilizes a single tube with  $180^\circ$  bends resting in the aluminum plate. This design will be simpler to manufacture and will not require a complex manifold simulation since the flow has only one path to flow through. The manifold design uses a machined fuel-rail to allow the fluid to flow through individual pipes. This design will require further investigation in order to determine the pressure needed to prevent any back flow into the tubing, but would ensure an even temperature across the tubing and plates. Similar to the two-dimensional cases, the temperature drop will be investigated across each of the tubing designs. If the eight

tube design also experiences a temperature drop of over 0.1K along the surface in three-dimensions, then it is known that the design will not be sufficient for the test setup.

### 5.2.1 Solution Domain

The tubing design was simulated in three-dimensions to capture the heat transfer and flow through the pipe to the plate. The study focused on the temperature drop across the entire surface of the aluminum plate. Thus, a single plate and tube assembly was investigated with the samples included. The other plate was substituted with an isothermal boundary condition to mimic the heat transfer expected. This provided the same result as running with the tubing, but required less computation time and overall file size.

### 5.2.2 Governing Equations, Boundary Conditions, and Initial Conditions

The conservation of energy, mass, and momentum in each direction, shown in Eq(5.3), Eq(5.4), and Eq(5.5) - Eq(5.7), are solved in the three-dimensional simulation.

Conservation of Energy

$$\rho C_p \left( u \frac{\partial T}{\partial x} + \frac{\partial T}{\partial y} + \frac{\partial T}{\partial z} \right) = k \left( \frac{\partial^2 T}{\partial x^2} + \frac{\partial^2 T}{\partial y^2} + \frac{\partial^2 T}{\partial z^2} \right) \quad (5.3)$$

Conservation of Mass

$$\frac{\partial u}{\partial x} + \frac{\partial v}{\partial y} + \frac{\partial w}{\partial z} = 0 \quad (5.4)$$



Conservation of Momentum in X-Direction

$$\rho \left( u \frac{\partial u}{\partial x} + v \frac{\partial v}{\partial y} + w \frac{\partial w}{\partial z} \right) = -\frac{\partial P}{\partial x} + \mu \left( \frac{\partial^2 u}{\partial x^2} + \frac{\partial^2 u}{\partial y^2} + \frac{\partial^2 u}{\partial z^2} \right) \quad (5.5)$$

Conservation of Momentum in Y-Direction

$$\rho \left( u \frac{\partial v}{\partial x} + v \frac{\partial v}{\partial y} + w \frac{\partial v}{\partial z} \right) = -\frac{\partial P}{\partial y} + \mu \left( \frac{\partial^2 v}{\partial x^2} + \frac{\partial^2 v}{\partial y^2} + \frac{\partial^2 v}{\partial z^2} \right) \quad (5.6)$$

Conservation of Momentum in Z-Direction

$$\rho \left( u \frac{\partial w}{\partial x} + v \frac{\partial w}{\partial y} + w \frac{\partial w}{\partial z} \right) = -\frac{\partial P}{\partial z} + \mu \left( \frac{\partial^2 w}{\partial x^2} + \frac{\partial^2 w}{\partial y^2} + \frac{\partial^2 w}{\partial z^2} \right) \quad (5.7)$$

In these equations, x, y, and z are the Cartesian coordinates, u, v, w are the velocity components in the x, y, and z-directions. T is the temperature and P is the pressure. The density is  $\rho$ , the thermal conductivity is k,  $C_p$  is the specific heat capacity, and  $\mu$  is the dynamic viscosity. In order to create the proper heat transfer model, the flow of a fluid is added inside the tubing. The fluid used is 50/50 mixture of water and ethylene glycol. The fluid is modeled as Newtonian and incompressible. The properties of the fluid are obtained from Matweb and shown in table 5.3. Materials from table 5.2 will also be reused for the samples, plates, and tubing in the simulation.

The flow rate will be specified by the mass flow rate through the inlet boundary condition of the tubing. Since the density of the fluid is known and the volumetric flow rate of the pump is given to be  $30 \frac{L}{min}$ , a simple conversion will yield the mass flow rate to be  $0.5385 \frac{kg}{s}$ . The flow was also assigned an isothermal condition of 318.15K to create the hot plate.

Table 5.3.: Ethylene glycol material properties obtained from MatWeb.

Material	Ethylene Glycol Solution (50/50)
Density $\rho$ [ $\frac{kg}{m^3}$ ]	1,077
Thermal Conductivity $k$ [ $\frac{W}{m \cdot K}$ ]	0.3
Specific Heat, $C_p$ [ $\frac{kJ}{kg \cdot K}$ ]	3,410
Dynamic Viscosity, $\mu$ [ $\frac{Ns}{m^2}$ ]	0.0028

In order to characterize the flow scheme, the Reynolds number must be calculated. Using Eq. 5.8, the Reynolds number was calculated to be 652, which is less than 10,000; validating that the liquid flow is laminar through the tubing.

$$R = \frac{4\dot{m}}{\mu\pi D} \quad (5.8)$$

The assembly exterior was assigned an adiabatic boundary condition treating it as fully insulated. This condition ensured that all of the heat transfer happened within the system and satisfied the conservation of energy. The hot plate was investigated and an isothermal boundary condition was given to the bottom of the HDPE sample to match the temperature of the cold plate, 281.15K. A schematic of the simulation can be seen in Figure 5.23.

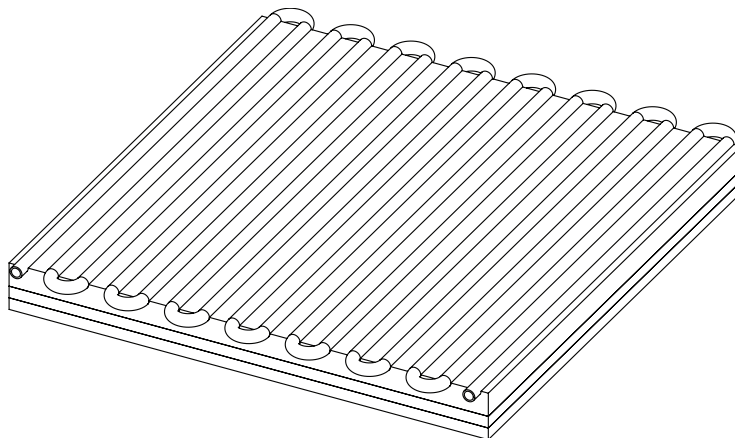


Figure 5.23.: Schematic of the 3D simulation assembly.

### 5.2.3 Solution Details

The flow simulation required the use of the on campus high performance computer, Rigel. Rigel is a 22 node, 288 core computer capable of running more computationally intense models. ANSYS CFX 16.0, another commercially available CFD solver, was used for the three-dimensional simulations. The mesh was created in Pointwise 17.3R5 and consisted of 5 blocks representing each separate component. Table 5.4 below displays the number of elements for each block and the number of elements used for the mesh independence study. The mesh sizing for the case and mesh independent study were spaced at 1.27mm (0.05in) and 0.635mm (0.025in). Temperature losses across the tube were compared and a maximum variance of less than 1.6% was seen.

Table 5.4.: Mesh independent study element count.

Volume Condition	Case Elements	Mesh Independent Study
Fluid	3,567,548	17,269,159
Tubing	3,329,290	15,595,475
Aluminum Plate	29,110,981	140,915,322
Stainless Steel	15,046,429	70,482,359
HDPE	15,074,402	71,825,519

#### 5.2.4 Results

The results from the three-dimensional case 4 simulation can be seen in Figure 5.24. What this shows is that the eight tube design is sufficient in providing the proper heat transfer to create an isothermal face with a single serpentine tube.

It can be seen that the maximum temperature variation between the inlet and outlet of the tubing is  $0.007^{\circ}\text{C}$ , which fulfills the required  $0.1^{\circ}\text{C}$  maximum temperature difference. It is important to note that the fully adiabatic boundary conditions simulated are not capable of being done with the facilities available. Therefore, it can be expected that the center of the face will be the best place to instrument in order to observe the isothermal condition.

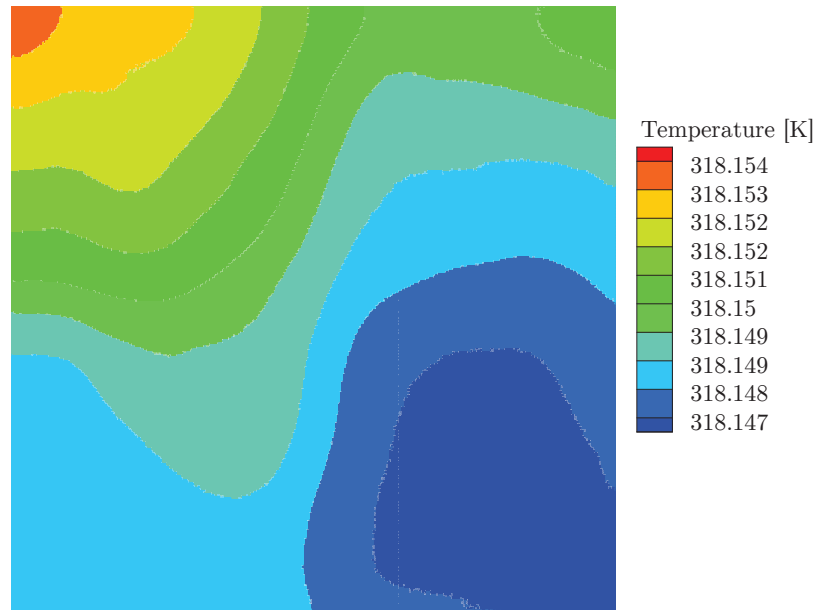


Figure 5.24.: Contour plot of hot plate surface temperatures.

### 5.3 Final Design

Using the data obtained from the two-dimensional and three-dimensional cases investigated, a final design of the Guarded Hot Plate Apparatus can be completed. The Mills design used copper plates and tubing for the hot and cold plates, instead of the aluminum being proposed with this study. Although copper has a higher thermal conductivity, aluminum is  $\frac{1}{3}$  the density and roughly  $\frac{2}{3}$  the cost of copper. With these in mind, the aluminum tubing and heat spreader plate was selected for the final design. The heat spreader plate is given a thickness of 25.4 mm (1.0 in) in order to effectively spread the heat from the tube to the samples. The samples to be used for the experiment will also be a 304 stainless steel plate for the known sample and the PCM-carbon fiber matrix for the unknown sample. The stainless steel is used since

the heat flux from the hot plate can be calculated through it due to all of the thermal properties being known. This then allows for the same calculation to be done on the unknown PCM sample resulting in the thermal conductivity to be determined.

Due to some manufacturing limitations, the simulated cases had to be modified in order to complete the design and manufacture of the test assembly. The tubing requirements were with the bends that suppliers were able to provide. In most cases, a one inch bend radius was the minimum bend that could be provided, thus the tubing was modified to have that bend radius resulting in a ten tube design for the cold and hot plates. The ten tube design yielded better cooling and heating effects than the eight tube, but needed a larger plate to house the tubing. The plates and sample sizes were also restricted to what was manufacturable within the campus CNC machines. The HAAS VF2 and VF3 CNC mill have a maximum table size of 30 inches in the x-direction and 20 inches in the y-direction. This restriction required that the plates be smaller and the design was modified to be 18in x 18in rather than the 20in x 20in used in the simulations. This size reduction had no effect on the heat transfer of the plates since the contact surface area was large enough. The final design for the cold and hot plate assembly can be seen in Figure 5.25.

The modified assembly was also simulated to test that the heat transfer was still within the requirements of the Guarded Hot Plate test. Figure 5.26 shows the results of the two-dimensional simulation conducted on the new tubing and plate design. It can be seen that the surface temperature is more uniform than the eight tube design with an maximum temperature variance of  $0.02^{\circ}\text{C}$  across the entire surface.

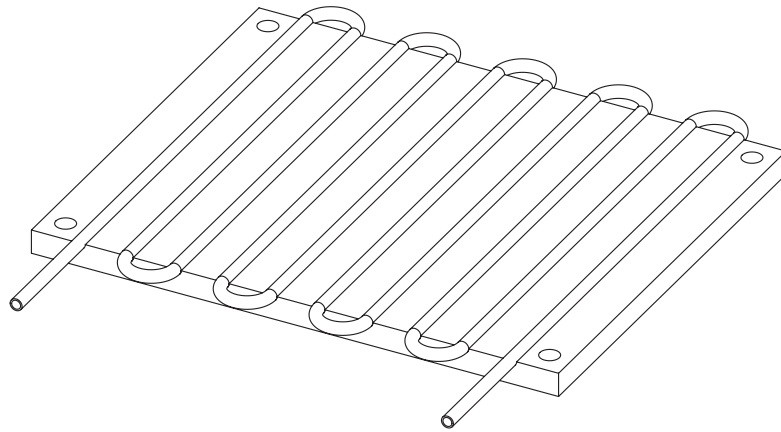


Figure 5.25.: Final design of the cold and hot plate.

Furthermore, a three-dimensional case was conducted following the case from above. As expected, the three-dimensional case also yielded a more steady temperature across the bottom of the aluminum plate with a max temperature differential of  $0.06^{\circ}\text{C}$ .

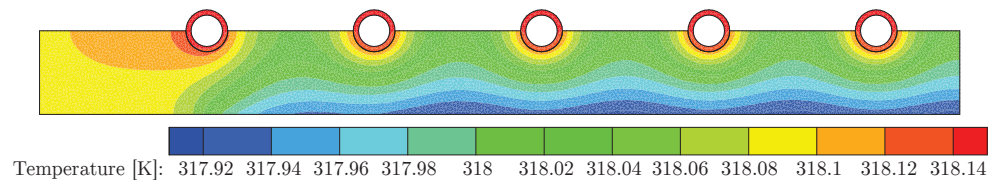


Figure 5.26.: Results from the 10 tube 2D simulation.

To complete the assembly of the test, the foam insulation must be simulated to determine the optimum number of sheets to use to minimize heat loss to the environment. The foam to be used are two inch thick pieces of DOW Styrofoam blue board with a thermal resistance value of 5 per inch. This foam has common use as insulation in houses and even structural core in composite components. The thermal conductivity of the foam is needed for the simulation. Using equation 5.9 seen below,

the thermal conductivity can be obtained with the thermal resistance,  $R$ , and the thickness of the material being known at 2 inches per sheet.

$$R = \frac{L}{k} \quad (5.9)$$

In the equation above,  $R$  is the thermal resistance,  $L$  is the thickness of the material, and  $k$  is the thermal conductivity. The foam simulation analyzed a single 2 inch (50.8mm) thick piece of styrofoam board. The left face of the foam was given an isothermal boundary from the hot plate set at 318.15K. The right face was given a convection boundary condition with the environment. The heat transfer coefficient of  $12.5 \frac{W}{m^2-K}$  and bulk ambient temperature of 293.15K was applied. The remaining faces were considered adiabatic. Figure 5.27 shows the simulation domain.

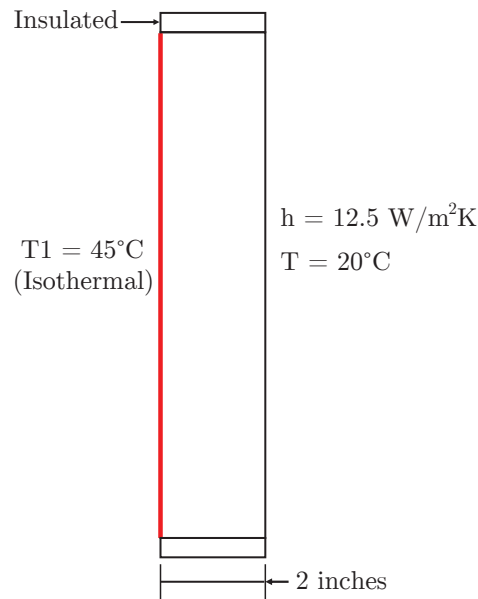


Figure 5.27.: Simulation domain for the foam study.



The simulation was conducted in ANSYS APDL 16.0 with two-dimensional heat transfer. The results from the simulation are shown in Figure 5.28. The temperature at the edge is seen to be 293.21K which is only 0.02% higher than ambient at 239.15K. This means that a single layer of two inch foam is sufficient in insulating the test setup from losing heat with the environment. A CAD image of the fully insulated test assembly is shown in Figure 5.29.

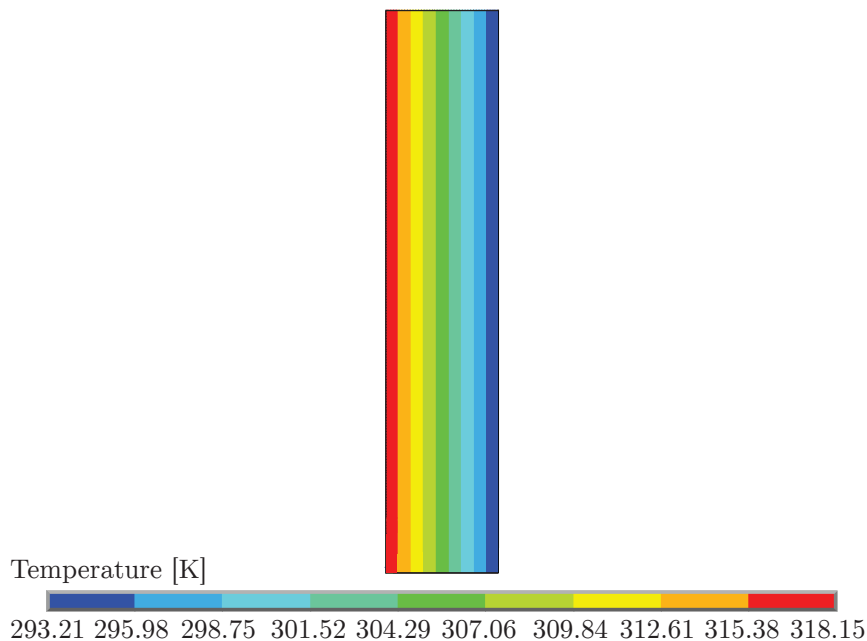


Figure 5.28.: Temperature contour seen through the thickness of the foam insulation.

To control the flow of ethylene glycol, two separate ANOVA A-40 constant temperature baths will be used to provide the isothermal boundary conditions for each plate. The baths will pump the fluid through the tubing creating the simple heat exchanger needed. Figure 5.30 shows the ANOVA A-40 used for these experiments.

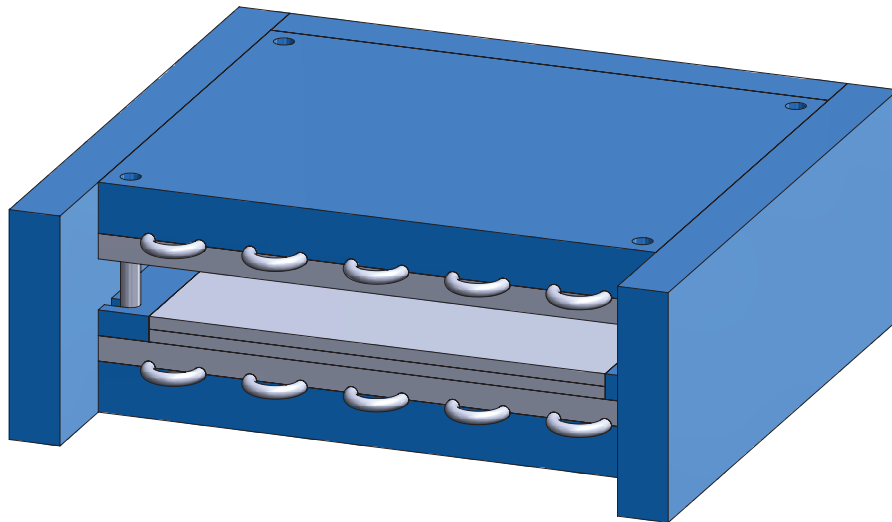


Figure 5.29.: CAD image of the steady state apparatus assembly.



Figure 5.30.: ANOVA A-40 used for the isothermal plates.

The tubing is brazed to the plates in order to create perfect thermal contact between them. Welding the two together would present a challenge and may cause

warping between the pieces. The tubing will also be flared on the free ends to a standard  $37^\circ$  allowing the use of an AN-8 tube nut to be placed on the end. The addition of the tube nut will provide a method of creating a mechanically sealed interface between the ANOVA A-40 constant temperature baths and the tubing. Thus the modified Guarded Hot Plate assembly is created and can be used to accurately determine the thermal conductivity of the PCM samples.

## **6. Implementation**

The PCM cold plate has been developed and now must be implemented to validate the feasibility with actual vehicle testing. The test platform to be used will be with the universities EcoCAR 3 team, the EcoEagles, and their 2016 Camaro.

### **6.1 EcoCAR 3 Competition**

EcoCAR 3 is a competition put on by the U.S. Department of Energy through their Advanced Vehicle Technology Competition series. The EcoCAR 3 competition focuses on taking the Chevrolet Camaro and redesigning it with innovative technology and a hybrid-electric powertrain. The purpose of the competition is to develop a vehicle that maintains the performance of a Camaro, while having reduced energy consumption with increased vehicle efficiency.

### **6.2 The Vehicle Test Platform**

The EcoEagles have designed a 2016 Eco Super Sport Camaro with a Parallel-Series Plug-in Hybrid Electric Vehicle (PHEV) powertrain architecture. This system uses a General Motors 2.4L Ecotec engine utilizing E85 as fuel. The engine is bolted directly to two Bosch IMG electric motors with clutches. These components drive

a General Motors 8L90 eight-speed automatic transmission followed by a differential on the rear wheels. The vehicle layout is shown in figure 6.1.

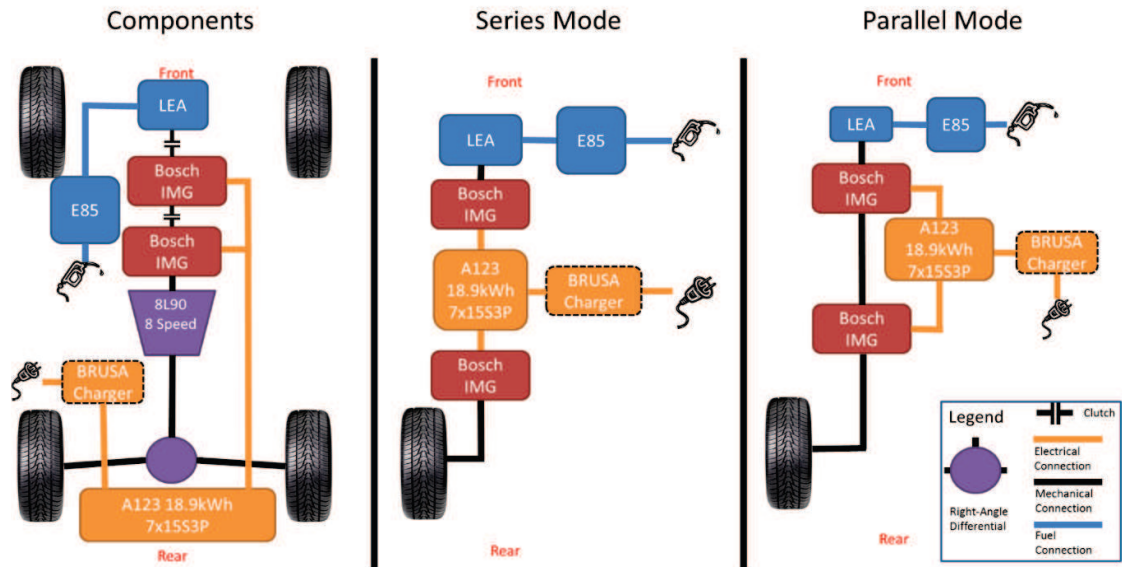


Figure 6.1.: ERAU Vehicle Architecture Selection.

### 6.2.1 PCM Implementation into ESS

The focus for implementation of the PCM cold plate will be with the vehicles ESS which uses seven A123 15S3P battery modules with a capacity of 18.9kWh operating at a nominal voltage of 350V. With this battery system, the powertrain can achieve 260kW of power and 890Nm of torque, resulting in a large amount of generated heat from the ESS.

For ease of packaging within the vehicle, the battery modules have been split into two groups each with their own PCM cold plate to capture the heat. An exploded

view of the ESS configuration can be seen in figure 6.2. Each tray is designed to house a 6.5 x 13.75 x 0.5 inch cold plate per battery foot print, resulting in seven complete cold plates capable of absorbing a total of 0.995MJ of energy combined.

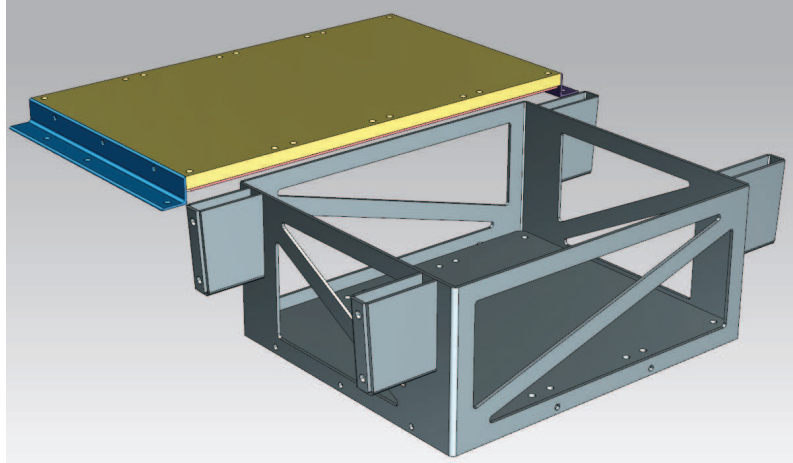


Figure 6.2.: ESS frame design with PCM cold plate trays attached.

### 6.2.2 PCM Plate Manufacture

The trays are manufactured from 6061-T6 aluminum and bolt directly to the ESS housing. This is to ensure the proper thermal contact required to remove the heat from the batteries. Additionally, a layer of Omega Thermal Paste is used to provide optimal heat conduction between the plates.

### 6.2.2.1 PCM Sealing

To contain the PCM within the enclosure, there are redundant seals of buna-N o-rings. Buna-N was selected based upon same accelerated life material compatibility test conducted with the PCM experiments. This accelerated life test was done with common sealing materials at a higher temperature, 50°C, to increase degradation of the sealing material over a shorter period of time to gauge the life cycle of the material. Furthermore, the corrosive nature of the PCM is mostly observed at higher temperatures.

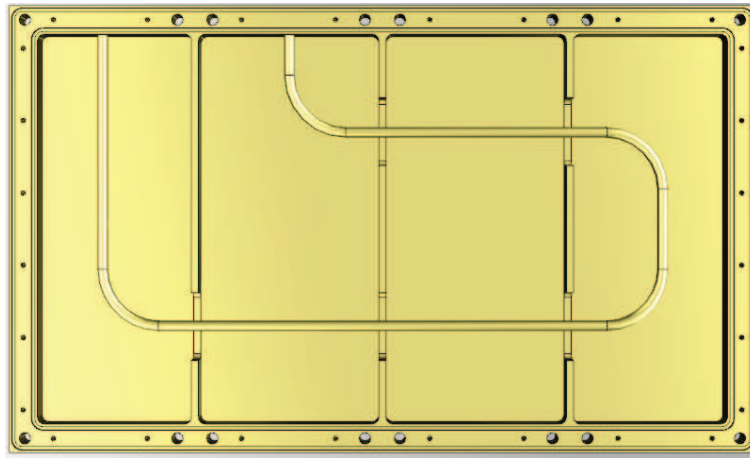


Figure 6.3.: Bottom PCM tray used on the vehicle ESS.

The materials selected were buna-N, silicone, and a cork seal infused with buna-N. Success of the seal was determined by visual inspection and possible failures with the seal when the test was concluded. From the test, buna-N showed the least amount of degradation over a 48 hour test. Both the silicone and cork were partially decayed due to the corrosive PCM and had several leak points. It was determined that the

buna-N seal would be work for a long term solution to sealing, however, it will still degrade and will need replacement. The total life was not determined, but is expected to outlive the components based upon visual inspections.

#### **6.2.2.2 Active Cooling Loop**

Following the EcoCAR 3 rules, an active cooling loop was added, although not necessary due to the high energy storage of the PCM, and functioned primarily as backup during prolonged test periods. The active system uses ethylene-glycol pumped through copper coils that are placed within the PCM trays to pull the heat away from saturated PCM in order to extend its use. The heat in the glycol is then put through a radiator and lost to the environment.

#### **6.2.3 Vehicle Testing Results**

This system has since been tested during the EcoCAR3 Year two competition and more recently at a test at Kennedy Space Center.. This test was done with the vehicle running in charge-deplete, charge-sustain, and sport mode. Data obtained from the onboard DAQ during charge depletion, shows that the PCM is capable of passively absorbing that latent heat energy without the use of an active cooling system. The test data is shown in Figure 6.4.



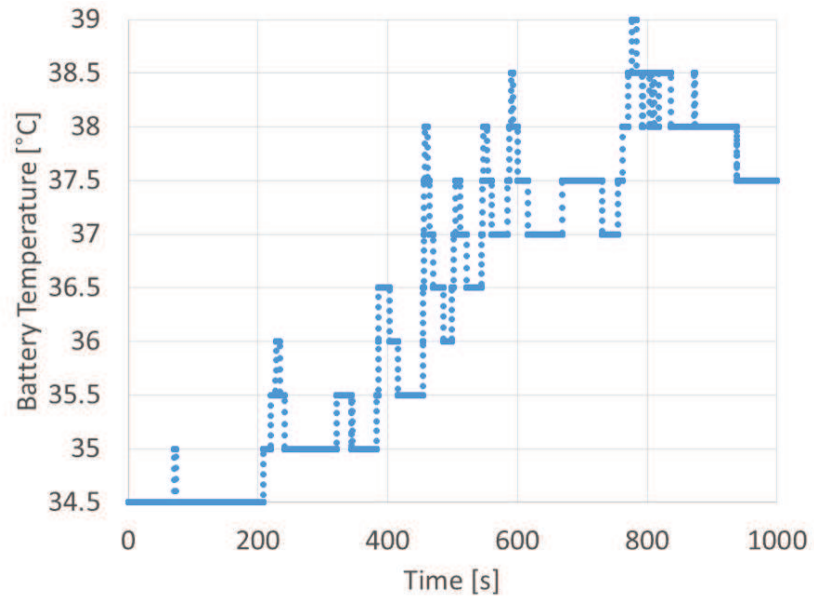


Figure 6.4.: ESS temperature data obtained during vehicle testing.

After an aggressive drive cycle, the maximum temperature observed in the ESS was 39°C proving that the cold plate is effective in keeping the temperature low, while not even activating the active cooling pump

## 7. Future Work

Due to the success of the innovative prototype design in EcoCAR3 Year 2, future studies will continue working with the team with manufacturing and implementation methods of a shape stabilized PCM cold plate. Shape stabilized PCM is unique due to the incorporation of a plastic material, commonly high density polyethylene (HDPE), to mix with the PCM in order to create a homogenous mixture that contains the melted PCM and provide rigid structure that requires no sealing. The same thermal conductivity enhancers, such as carbon fibers, can be mixed in during manufacture to yield a shape-stabilized composite cold plate with higher thermal conductivity similar to the standard PCM cold plate.

### 7.1 Shape Stabilized PCM

Shape stabilization of PCM was first introduced in 1985 by Feldman et al [(Feldman, Shapiro, & Fazio, 1985)] who investigated ways of manufacturing PCM tiles for thermal storage. He used different plastics such as PVC, PVA, and HDPE to create the shape stabilized plate for use in building walls and floors for heating and cooling purposes. This innovation was then modified with thermal conductivity enhancers due to the naturally low thermal conductivity of the PCM by Cheng et al [(W.-L. Cheng, Zhang, Xie, Liu, & Wang, 2010), (W. Cheng, Xie, Zhang, Xu, & Xia, 2015)] who

mixed expanded graphite fibers into the HDPE-PCM mixture. The same researchers have validated the use of their tiles in 2015 by implementing the plates in the floor of a home for heat storage during winter. However, this is the first instance of this technology being implemented into thermal management of EV and HEV systems.

Using the Guarded Hot Plate, the shape-stabilized cold plate must be thermally characterized in order to determine the effect the carbon fiber and HDPE additions. Once characterized, the manufacturing process can be investigated. A benefit of the shape-stabilization lies within the manufacturing capabilities of being printed, molded, and extruded due to the plastic stabilizer and PCM liquid phase. This property also allows for it to be packaged and implemented onto the vehicle without geometric restrictions. focus specifically on the molding and casting process of shape-stabilized PCM-composite cold plate.

## **7.2 Wax Material Study**

It has been discovered that the PCM-37 used with the previous experiments will be incapable of being used for the shape stabilization. This is because, according the PureTemp, PCM-37 will fully break down at temperatures over 50°C higher than the melt point. Since HDPE has a melt point of 160°C, an alternative must be used. A common material to be mixed is paraffin wax. Thus a material study of three different waxes, paraffin, bee's, and soy wax, have been conducted to determine the best choice for mixing with the HDPE.

Using the Mettler Toledo Differential Scanning Calorimeter (DSC), the latent heat of fusion and onset melt temperatures, are capable of being determined. Figure 7.1 shows the Mettler Toledo DSC-3 used for the experiments. A comparison between the waxes' thermal properties will help in selecting the best base wax for mixing with HDPE. Ideally, the best wax will have a melt temp closest to PCM-37 with a high latent heat of fusion, however, it is expected to be lower than the PCM-37.



Figure 7.1.: Mettler Toledo Differential Scanning Calorimeter.

The experiments conducted follow a custom scheme developed on the DSC that is designed for testing waxes with melting points between 40 and 60°C. The scheme has five segments to characterize the material. First the test chamber on the instrument will go to 20°C and rest for 10 minutes to normalize the specimens. The second segment will heat from 20°C to 90°C at a 2°C per minute heat rate. This heat rate will provide enough resolution to witness the melt curves of each of the waxes. The test will then sit at 90°C for five minutes and go back down to 20°C at the same rate.

### 7.2.1 Results

The test was conducted at a minimum of three times per material until the data was correlated. The first material explored is the paraffin wax, which is used commonly investigated for shape-stabilized PCM plates. The bees wax and soy wax, although not commonly used, were comparisons that were commercially available during the time of the study. The materials specimen used were first weighed in a Mettler Toledo scale to determine the sample mass. The masses are shown in table 7.1 of each wax sample.

Table 7.1.: Wax sample masses used for the DSC experiments.

Wax	Mass [mg]
Paraffin Wax	5.95
Bees Wax	12.90
Soy Wax	11.15

The wax samples were placed in  $40\mu\text{L}$  crucibles designed specifically for the DSC. Air is used as a reference for the experiments.

To obtain the data from the experiment, each segment of the test is separated. The data needed is observed within the second segment when the wax material is melted. A comparison between the three materials during segment two can be seen in figure 7.2. This data reflects the averages of each material over the completed experiments.

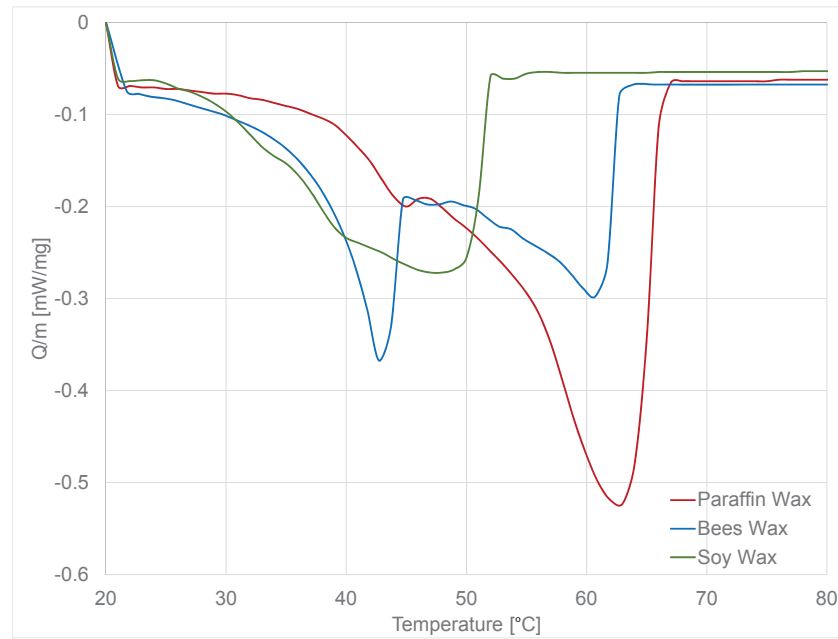


Figure 7.2.: Melt curves of the three sample waxes.

To obtain the necessary data, the curve is integrated providing the energy absorbed, or latent heat of fusion, during the heating process. The onset and peak melt temperatures are calculated from the largest peak of the melt curve. Table 7.2 shows the data gained from the experiments for each wax.

Table 7.2.: Properties obtained from DSC sample testing.

Property	Paraffin Wax	Bees Wax	Soy Wax
Latent Heat of Fusion [ $\frac{J}{g}$ ]	185.4	147.9	102.1
Onset Melt Temperature [ $^{\circ}C$ ]	50.8	37.6	31.2
Peak Melt Temperature [ $^{\circ}C$ ]	62.6	43.3	47.5

From the data, it is clear that the best wax to use for further experiments will be a paraffin wax with a specific melt temperature. This is due to the higher latent heat of fusion even though the melt range is higher than what is needed for the vehicle ESS thermal management. The next step will involve mixing the HDPE stabilizer to create a prototype shape-stabilized PCM cold plate and conduct further characterization experiments. These experiments will determine the feasibility of the technology for use with vehicle implementation and provide data for the possible addition of thermal conductivity enhancers. Furthermore, the prototype will provide insight in the manufacture and development of the shape-stabilized PCM cold plates for future testing and use.

## REFERENCES

- Al Hallaj, S., & Selman, J. (2000). Novel thermal management system for electric vehicle batteries using phase-change material. *Journal of the Electrochemical Society*, 147, 3231-3236.
- Al-Hallaj, S., & Selman, J. (2002). Thermal modeling of secondary lithium batteries for electric vehicle/hybrid electric vehicle applications. *Journal of Power Sources*, 110, 341-348.
- ASTM International, ASTM C177-13 [Online]. Available: <http://www.astm.org/Standards/C177>
- Barsotti, D. L., & Boetcher, S. (2014). Novel battery cold plate design for increase passive cooling. In SAE technical paper 2014-01-1919.
- Battery University, Types of Lithium-Ion [Online]. Available: [batteryuniversity.com/learn/article/types\\_of\\_lithium\\_ion](http://batteryuniversity.com/learn/article/types_of_lithium_ion)
- Battery University, How do Lithium-Ion Batteries Work? [Online]. Available: [batteryuniversity.com/learn/article/types\\_of\\_lithium\\_ion](http://batteryuniversity.com/learn/article/types_of_lithium_ion)
- Buford, K., Williams, J., & Simonini, M. (2011). Determining most energy efficient cooling control strategy of a rechargeable energy storage system.
- Cheng, W., Xie, B., Zhang, R., Xu, Z., & Xia, Y. (2015). Effect of thermal conductivities of shape stabilized PCM on under-floor heating system. *Applied Energy*, 144, 10-18.
- Cheng, W.-L., Zhang, R.-M., Xie, K., Liu, N., & Wang, J. (2010). Heat conduction enhanced shape-stabilized paraffin/hdpe composite pcms by graphite addition: Preparation and thermal properties. *Solar Energy Materials and Solar Cells*, 94 (10), 1636-1642. (cited By 79)
- Chintakrinda, K., Warzoha, R. J., & Weinstein, A. S., R. D. abd Fleisher. (2012). Quantification of the impact of embedded graphite nano fibers on the transient thermal response of paraffin phase change material exposed to high heat fluxes. *ASME Journal of Heat Transfer*, 134 (7), 071901-071901-10.
- Chintakrinda, K., Weinstein, R. D., & Fleischer, A. S. (2011). A direct comparison of three different material enhancement methods on the transient thermal response of paraffin phase change material exposed to high heat fluxes. *International Journal of Thermal Sciences*, 50 (9), 1639-1647.
- Elgafy, A., & Lafdi, K. (2005). Effect of carbon nano fiber additives on thermal behavior of phase change materials. *Carbon*, 43 (15), 3067 - 3074.



- Environmental Protection Agency, Evolution of the Pollution Control Act [Online] Available: <https://www.epa.gov/clean-air-act-overview/evolution-clean-air-act>
- Feldman, D., Shapiro, M., & Fazio, P. (1985). A heat storage module with a polymer structural matrix. *Polymer Engineering & Science*, 25 (7), 406-411. (cited By 26)
- Fukai, J., Kanou, M., Kodama, Y., & Miyatake, O. (2000). Thermal conductivity enhancement of energy storage media using carbon fibers. *Energy Conversion and Management*, 41 (14), 1543-1556.
- Hamdan, M., & Elwerr, F. (1996). Thermal energy storage using a phase change material. *Solar Energy*, 56 (2), 183 - 189.
- Humphries, G. E. I., W. R. (1977). A design handbook for phase change thermal control and energy storage devices. NASA Technical Paper 1074.
- Khateeb, S. A., Farid, M. M., Selman, J., & Al-Hallaj, S. (2004). Design and simulation of a lithium-ion battery with a phase change material thermal management system for an electric scooter. *Journal of Power Sources*, 128, 292 - 307.
- Kim, G.-H., Gonder, J., Lustbader, J., & Pesaran, A. (2008). Thermal management of batteries in advanced vehicles using phase-change materials. *The World Electric Vehicle Journal*, 2, 46-59.
- Kizilel, R., Sabbah, R., Selman, J. R., & Al-Hallaj, S. (2009). An alternative cooling system to enhance the safety of li-ion battery packs. *Journal of Power Sources*, 194, 1105 - 1112.
- Mills, A., & Al-Hallaj, S. (2005). Simulation of passive thermal management system for lithium-ion battery packs. *Journal of Power Sources*, 141, 307 - 315.
- Mills, A., Farid, M., Selman, J., & Al-Hallaj, S. (2006). Thermal conductivity enhancement of phase change materials using a graphite matrix. *Applied Thermal Engineering*, 26, 1652 - 1661.
- Onda, K., Ohshima, T., Nakayama, M., Fukuda, K., & Araki, T. (2006). Thermal behavior of small lithium-ion battery during rapid charge and discharge cycles. *Journal of Power Sources*, 158 (1), 535 - 542.
- Park, S., & Jung, D. (2010). Design of vehicle cooling system architecture for a heavy duty series-hybrid electric vehicle using numerical system simulations. *Journal of Engineering for Gas Turbines and Power*, 132.
- Sabbah, R., Kizilel, R., Selman, J., & Al-Hallaj, S. (2008). Active (air-cooled) vs. passive (phase change material) thermal management of high power lithium-ion packs Limitation of temperature rise and uniformity of temperature distribution. *Journal of Power Sources*, 182 (2), 630 - 638.

- Sato, N. (2001). Thermal behavior analysis of lithium-ion batteries for electric and hybrid vehicles. *Journal of Power Sources*, 99 (12), 70 – 77
- Shamsundar, N., & Sparrow, E. (1975). Analysis of multidimensional conduction phase change via the enthalpy model. *ASME Journal of Heat Transfer*, 97, 333-340.